

Nonlinear Power Spectrum from Resummed Perturbation Theory: a Leap Beyond the BAO Scale

Stefano Anselmi

Institut de Ciències de l'Espai, IEEC-CSIC, Campus UAB,
Facultat de Ciències, Torre C5 par-2, Barcelona 08193, Spain

E-mail: anselmi@ieec.uab.es

Massimo Pietroni

INFN, Sezione di Padova, via Marzolo 8, I-35131, Padova, Italy

E-mail: massimo.pietroni@pd.infn.it

Abstract. A new computational scheme for the nonlinear cosmological matter power spectrum (PS) is presented. It allows an analytic summation, at all orders in perturbation theory, of the leading contributions at small scales, thus extending to the PS the program initiated by Crocce and Scoccimarro for the nonlinear propagator. Our method is based on evolution equations in time, which can be cast in a form extremely convenient for fast numerical evaluations. A nonlinear PS is obtained in a time comparable to that needed for a simple 1-loop computation, and the numerical implementation is very simple. Our results agree with N-body simulations at the percent level in the BAO range of scales, and at the few-percent level up to $k \simeq 1 \text{ h/Mpc}$ at $z \gtrsim 0.5$, thereby opening the possibility of applying this tool to scales interesting for weak lensing. We clarify the relation between our approach and previous ones, such as the Time Renormalization Group, and the multi-point propagator expansion. We discuss possible lines of improvements of the method and its intrinsic limitations by multi streaming at small scales and low redshifts.

1. Introduction

Cosmological perturbation theory (PT) as a tool to study the Large Scale Structure of the Universe (LSS) (for a review see [1]) has received considerable interest in the recent past. The main motivation is the study of Baryonic Acoustic Oscillations (BAO) imprinted in the matter power spectrum (PS), which are one of the main observables of present and future galaxy surveys [2, 3, 4, 5, 6, 7, 8, 9, 10]. The goal of these measurements is to derive the acoustic scale at the percent level accuracy, in order to provide constraints on the Dark Energy equation of state competitive with those obtained from measurements of the magnitude-redshift relation of type Ia Supernovae [11, 12]. Of course, on the theory side, the matter PS in the BAO range of scales ($\simeq 100$ Mpc/h) must be computed at the same level. For a Λ CDM cosmology, the goal can be accomplished by means of high accuracy N-body simulations, once the various issues related to precise initial conditions, very large simulation volumes, mass resolution and time stepping are carefully addressed, as discussed, *e.g.*, in [13]. However, the long computational times required by these simulations make it impossible to implement grid based or Markov Chain Monte Carlo (MCMC) estimations of cosmological parameters, which typically require the evaluation of thousands of PS's. Moreover, if departures from Λ CDM cosmologies are taken into account, for instance by the inclusion of massive neutrinos, non gaussian initial conditions, or $f(R)$ theories of gravity, the N-body approach is still far from being firmly established at the percent level in the relevant range of scales.

The usage of PT can potentially help in most of these respects. First, being based on analytic, or semi-analytic, techniques, computational times are in general greatly reduced with respect to N-body simulations. Moreover, although the basic formalism is derived for an Einstein-de Sitter cosmology, its extension to Λ CDM is straightforward, and also its formulations in non-standard cosmologies are feasible and under control [14, 15, 16, 17, 18, 19]. However, the real boost to these methods was given by the papers of Crocce and Scoccimarro (CS) [20, 21], who showed how the poorly behaving PT series can be reorganized, in what they named “renormalized PT” (RPT), in such a way as to obtain a better behaved expansion, valid in a larger range of scales. In particular, they showed that a certain quantity, namely the propagator defined in eq. (18), which measures the sensitivity of density and velocity perturbations to a variation in their initial conditions, can be computed *exactly, i.e.* at all orders in PT, in the large wavevector k (small scale) limit. CS finding prompted a certain number of independent investigations on possible ways to resum PT contributions at all orders, both for the propagator [22, 23, 24, 25], and for the directly measurable PS [14, 26, 27, 28, 29, 30, 31, 32]. An alternative method, having the Zeldovich approximation as starting point, was proposed in [33, 34]. The status of these methods to date can be summarized as follows: at $z \gtrsim 1$ the PS can be computed at a few percent accuracy (in comparison with state of the art N-body simulations) in the BAO range of scales ($0.05 \lesssim k \lesssim 0.25$ h/Mpc), the accuracy degrading quite rapidly at higher

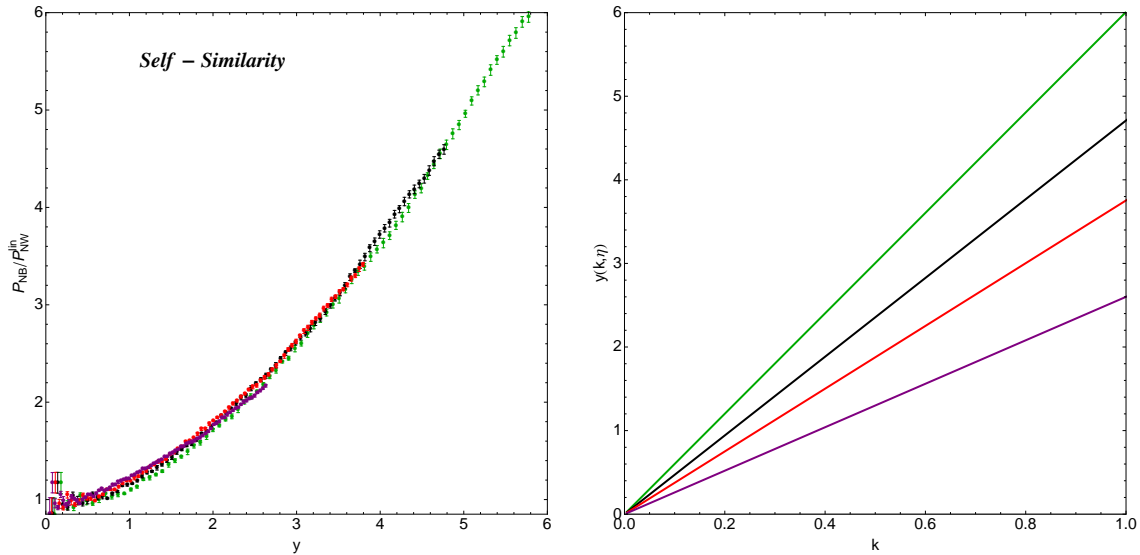


Figure 1. (left) The nonlinear PS from the N-body simulations of [35], divided by the no-wiggle PS of [36], plotted against the variable y defined in eq. (1). The color-code is the following: green for $z = 0$, black for $z = 0.5$, red for $z = 1$, and purple for $z = 2$. Each PS has been truncated at $k = 1 \text{ h/Mpc}$. (right) The relation between y and k at different redshifts.

wave numbers (smaller scales) and smaller redshifts. Moreover, the computational time of these approaches, though much smaller than for N-body simulations, is still in the few hours range for a single PS, thereby making the implementations of MCMC's still quite problematic.

In this paper we present a new computational scheme which overcomes the present limitations of resummed PT approaches in both respects: it greatly enlarges the range of scales in which it gives results accurate at the percent level, and it greatly reduces computational times. At $z = 1$ we can compute the PS up to $k \simeq 1 \text{ h/Mpc}$ at the percent level, in a time comparable to that of a simple 1-loop computation, namely, $O(1)$ minutes. This opens the road both to parameter estimation via MCMCs, and to the extension of these kind of methods from the BAO physics to weak lensing measurements.

At the technical level, our main result is an exact resummation of the leading PT corrections to the PS in the large k limit. In the CS resummation for the propagator the effective expansion parameter in the large k limit turns out to be [21]

$$y \equiv e^\eta \sigma_v k, \quad (1)$$

where $\eta = \log D(z)/D(z_{in})$ ($D(z)$ being the linear growth factor), and

$$\sigma_v^2 \equiv \frac{1}{3} \int d^3q \frac{P^0(q)}{q^2}, \quad (2)$$

with $P^0(q)$ the linear PS evaluated at the initial redshift, to be formally sent to infinity (in practice, in this paper we will use $z_{in} = 100$). Our starting point is the realization that, in the small scale limit, also the PS becomes a function of the variable y defined

in eq. (1). In Fig. 1 we plot the PS from the N-body simulations of [35] at different redshifts, normalized by the smooth PS by Eisenstein and Hu [36], as a function of y . It is clear that, for $y > O(1)$, all the PS's can be expressed as an universal function depending on y alone. Therefore our goal is to identify, at each order in PT, the leading large y corrections which, once resummed at all orders, give the y -function plotted in Fig. 1. In the extreme large y limit, it is given by the simple analytic expression in eq. (50), which in the range of scales considered in this paper ($k \lesssim 1 \text{ h/Mpc}$) is corrected by the solution of eq. (33) discussed in sects. 6 and 7.

We formulate a very efficient way to reorganize the PT expansion, based on evolution equations in time which are exact at all orders in PT. A similar approach was already presented in ref. [22] for the propagator, where it was used to reproduce the CS result, and also to include next-to-leading corrections. Here we derive the relevant equation for the PS and, after implementing the same approximation leading to the CS result, we derive its limiting behavior in the large k or, better, large y , limit. At the same time, at low k , the equation is solved by the 1-loop PS, thereby providing an interpolation between the two correct behaviors in the two extremes of the physically interesting range of scales. The equation contains two kinds of kernel functions. One is the same entering the equation for the propagator, and was already discussed in ref. [22]. A computation of this kernel function at 1-loop provides, by virtue of our evolution equation, the CS propagator at all loop order, as well as part of the leading corrections to the PS. The resummation of the leading corrections of the remaining part, which is responsible for mode-mode coupling, is the main result of this paper.

As we have already anticipated, our resummation procedure works remarkably well: its performance degrades only for (low) redshifts and (small) scales where the effect of multi-streaming, the intrinsic limit of eulerian PT, is known to become relevant [37, 38]. In other words, we can claim that, at the few percent level, our approach takes into account all the physics contained in the Euler-Poisson system on which eulerian PT is founded. As a consequence, it provides the best starting base for methods aimed at going beyond the single-stream approximation, as that proposed in [39].

The paper is organized as follows. In sec. 2 we review eulerian PT in the compact form discussed in [21, 26], the diagrammatic approach to the PT expansion, and we recall the exact expressions for the fully nonlinear propagator and PS, which provide the starting points for their evolution equations. In sec. 3 we derive the evolution equations for the propagator and for the PS, and their approximate expressions in the large and small k limit. In sec. 4 we show how, in the $k \rightarrow 0$ limit, the PS equation is solved by the standard 1-loop expression for the PS, and in sec. 5 we discuss how a simple upgrading of the 1-loop expression provides an all-order resummation valid in the small k regime. Then, in sec. 6 we derive the main result of this paper, namely the large k resummation for the mode-mode coupling part of the PS evolution, and also an approximate analytic expression for the PS in the same limit. In sec. 7 we discuss how to interpolate between the small and large k regimes discussed in the previous sections, and in sec. 8 we present our numerical results and their comparison with N-body simulations. Finally, in sec. 9

we discuss our results and possible developments.

In Appendix A and Appendix B we give explicit formulas for the numerical implementation of the method.

2. Nonlinear fluid equations and perturbation theory

Eulerian PT [1] aims at solving the system of three fluid equations: continuity, Euler, Poisson. Starting from the case of Einstein-de Sitter cosmology, the equations can be written as follows

$$\begin{aligned} \frac{\partial \delta_m}{\partial \tau} + \nabla \cdot [(1 + \delta_m)\mathbf{v}] &= 0, \\ \frac{\partial \mathbf{v}}{\partial \tau} + \mathcal{H}\mathbf{v} + (\mathbf{v} \cdot \nabla)\mathbf{v} &= -\nabla\phi, \\ \nabla^2\phi &= \frac{3}{2}\mathcal{H}^2\delta_m, \end{aligned} \quad (3)$$

where $\mathcal{H} = d \log a / d\tau$ is the Hubble Parameter in conformal time, while $\delta_m(\mathbf{x}, \tau)$ and $\mathbf{v}(\mathbf{x}, \tau)$ are the DM number-density fluctuation and the DM peculiar velocity field, respectively.

Defining, as usual, the velocity divergence $\theta(\mathbf{x}, \tau) = \nabla \cdot \mathbf{v}(\mathbf{x}, \tau)$, and going to Fourier space, the equations in (3) can be expressed as

$$\begin{aligned} \frac{\partial \delta_m(\mathbf{k}, \tau)}{\partial \tau} + \theta(\mathbf{k}, \tau) \\ + \int d^3\mathbf{q} d^3\mathbf{p} \delta_D(\mathbf{k} - \mathbf{q} - \mathbf{p}) \alpha(\mathbf{q}, \mathbf{p}) \theta(\mathbf{q}, \tau) \delta_m(\mathbf{p}, \tau) &= 0, \\ \frac{\partial \theta(\mathbf{k}, \tau)}{\partial \tau} + \mathcal{H}\theta(\mathbf{k}, \tau) + \frac{3}{2}\mathcal{H}^2\delta_m(\mathbf{k}, \tau) \\ + \int d^3\mathbf{q} d^3\mathbf{p} \delta_D(\mathbf{k} - \mathbf{q} - \mathbf{p}) \beta(\mathbf{q}, \mathbf{p}) \theta(\mathbf{q}, \tau) \theta(\mathbf{p}, \tau) &= 0. \end{aligned} \quad (4)$$

The nonlinearity and non-locality of the fluid equation are encoded in the two functions

$$\alpha(\mathbf{q}, \mathbf{p}) = \frac{(\mathbf{p} + \mathbf{q}) \cdot \mathbf{q}}{q^2}, \quad \beta(\mathbf{q}, \mathbf{p}) = \frac{(\mathbf{p} + \mathbf{q})^2 \mathbf{p} \cdot \mathbf{q}}{2p^2q^2}, \quad (5)$$

which couple different modes of density and velocity fluctuations.

One can write Eqs. (4) in a compact form [21]. First, we introduce the doublet φ_a ($a = 1, 2$), given by

$$\begin{pmatrix} \varphi_1(\mathbf{k}, \eta) \\ \varphi_2(\mathbf{k}, \eta) \end{pmatrix} \equiv e^{-\eta} \begin{pmatrix} \delta_m(\mathbf{k}, \eta) \\ -\theta(\mathbf{k}, \eta)/\mathcal{H} \end{pmatrix}, \quad (6)$$

where the time variable has been replaced by the logarithm of the scale factor,

$$\eta = \log \frac{a}{a_{in}},$$

a_{in} being the scale factor at a conveniently remote epoch, in which all the relevant scales are well inside the linear regime.

Then, we define a *vertex* function, $\gamma_{abc}(\mathbf{k}, \mathbf{p}, \mathbf{q})$ ($a, b, c, = 1, 2$) whose only independent, non-vanishing, elements are

$$\begin{aligned}\gamma_{121}(\mathbf{k}, \mathbf{p}, \mathbf{q}) &= \frac{1}{2} \delta_D(\mathbf{k} + \mathbf{p} + \mathbf{q}) \alpha(\mathbf{p}, \mathbf{q}), \\ \gamma_{222}(\mathbf{k}, \mathbf{p}, \mathbf{q}) &= \delta_D(\mathbf{k} + \mathbf{p} + \mathbf{q}) \beta(\mathbf{p}, \mathbf{q}),\end{aligned}\quad (7)$$

and $\gamma_{121}(\mathbf{k}, \mathbf{p}, \mathbf{q}) = \gamma_{112}(\mathbf{k}, \mathbf{q}, \mathbf{p})$.

The two equations (4) can now be rewritten in a compact form as

$$\partial_\eta \varphi_a(\mathbf{k}, \eta) = -\Omega_{ab} \varphi_b(\mathbf{k}, \eta) + e^\eta \gamma_{abc}(\mathbf{k}, -\mathbf{p}, -\mathbf{q}) \varphi_b(\mathbf{p}, \eta) \varphi_c(\mathbf{q}, \eta), \quad (8)$$

where

$$\Omega = \begin{pmatrix} 1 & -1 \\ -\frac{3}{2} & \frac{3}{2} \end{pmatrix}. \quad (9)$$

Repeated indices are summed over, and integration over momenta \mathbf{q} and \mathbf{p} is understood.

To extend the validity of this approach to Λ CDM, we will reinterpret the variable η as the logarithm of the linear growth factor of the growing mode, i.e. [1, 21, 14],

$$\eta = \ln(D/D_{in}), \quad (10)$$

and we redefine the field in Eq. (6) as

$$\begin{pmatrix} \varphi_1(\mathbf{k}, \eta) \\ \varphi_2(\mathbf{k}, \eta) \end{pmatrix} \equiv e^{-\eta} \begin{pmatrix} \delta_m(\mathbf{k}, \eta) \\ -\theta(\mathbf{k}, \eta)/\mathcal{H}f \end{pmatrix}, \quad (11)$$

with $f = d \ln D / d \ln a$. As discussed in [14], the above approximation is accurate at better than 1% level in the whole range of redshifts and scales we are interested in.

If we consider the linear equations (obtained in the $e^\eta \gamma_{abc} \rightarrow 0$ limit) we can define the *linear retarded propagator* as the operator giving the evolution of the field φ_a from η_{in} to η ,

$$\varphi_a^0(\mathbf{k}, \eta) = g_{ab}(\eta, \eta_{in}) \varphi_b^0(\mathbf{k}, \eta_{in}), \quad (12)$$

where the “0” index stands for the linear approximation to the full solution. The linear propagator obeys the equation

$$(\delta_{ab} \partial_\eta + \Omega_{ab}) g_{bc}(\eta, \eta_{in}) = \delta_{ac} \delta_D(\eta - \eta_{in}). \quad (13)$$

with causal boundary conditions. It is given explicitly by the following expression [21],

$$g_{ab}(\eta, \eta') = \left[\mathbf{B} + \mathbf{A} e^{-5/2(\eta - \eta')} \right]_{ab} \theta(\eta - \eta'), \quad (14)$$

with θ the step-function, and

$$\mathbf{B} = \frac{1}{5} \begin{pmatrix} 3 & 2 \\ 3 & 2 \end{pmatrix} \quad \text{and} \quad \mathbf{A} = \frac{1}{5} \begin{pmatrix} 2 & -2 \\ -3 & 3 \end{pmatrix}. \quad (15)$$

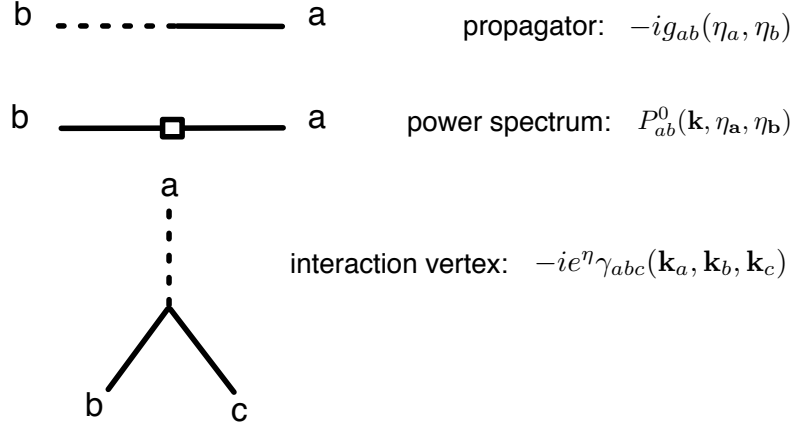


Figure 2. The Feynman Rules for cosmological perturbation theory

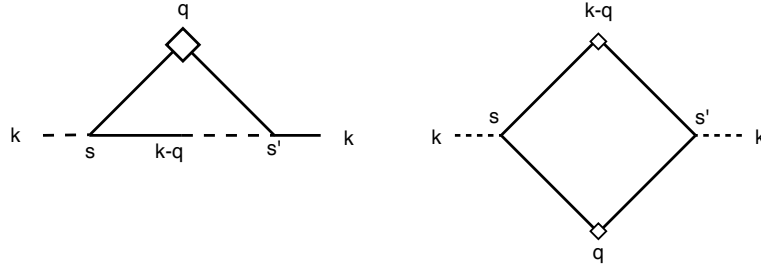


Figure 3. The two 1PI functions $\Sigma_{ab}^{(1)}$ and $\Phi_{ab}^{(1)}$ at 1-loop, given explicitly by eqs. (A.1) and (A.3).

The growing ($\varphi_a \propto \text{const.}$) and the decaying ($\varphi_a \propto \exp(-5/2(\eta - \eta'))$) modes can be selected by considering initial fields φ_a proportional to

$$u_a = \begin{pmatrix} 1 \\ 1 \end{pmatrix} \quad \text{and} \quad v_a = \begin{pmatrix} 1 \\ -3/2 \end{pmatrix}, \quad (16)$$

respectively.

In the following, we will be interested in the PS

$$\langle \varphi_a(\mathbf{k}, \eta) \varphi_b(\mathbf{k}', \eta') \rangle \equiv \delta_D(\mathbf{k} + \mathbf{k}') P_{ab}(k; \eta, \eta'), \quad (17)$$

and in the propagator,

$$\left\langle \frac{\delta \varphi_a(\mathbf{k}, \eta)}{\delta \varphi_b(\mathbf{k}', \eta')} \right\rangle \equiv i \delta_D(\mathbf{k} + \mathbf{k}') G_{ab}(k; \eta, \eta'), \quad (18)$$

which gives the response of the field at time η to a change in the field at an earlier time $\eta' < \eta$. The linear approximations of the fully nonlinear quantities above are given by the linear PS

$$P_{ab}^0(k; \eta, \eta') = g_{ac}(\eta, \eta_{in}) g_{bd}(\eta, \eta_{in}) P_{cd}^0(k; \eta_{in}, \eta_{in}), \quad (19)$$

and by the linear propagator $g_{ab}(\eta, \eta')$ of eq. (14), respectively.

These quantities, as well as all higher order correlation functions, can be computed perturbatively by solving iteratively the nonlinear equations (8), supplemented by the initial conditions at the time η_{in} for the PS, the bispectrum, and, in principle, all higher correlation functions. In this paper, we will limit ourselves to the case of gaussian initial conditions, and therefore we will assume that the initial conditions are fully characterized by the PS only. A very convenient way to organize the perturbative expansion is to use the diagrammatic language discussed in [20] and in [26] (for details on the derivation of formalism used in this paper, the reader is referred to the latter). The building blocs are given in Fig. 2, and are the linear propagator, the linear PS, and the interaction vertex of eq. (7). Propagators and PS can only be joined according to the rule encoded in the vertex, *i.e.*, two continuous ends join with a dashed one. Notice, moreover, that according to eq. (19), a linear PS can be seen as the initial PS, represented by the empty square in Fig. 2, sandwiched between two linear propagators. This will be useful in the following.

The full nonlinear PS and propagator have the following structures [26]

$$\begin{aligned}
 P_{ab}(k; \eta, \eta') &= G_{ac}(k; \eta, \eta_{in}) G_{bd}(k; \eta', \eta_{in}) P_{cd}(k; \eta_{in}, \eta_{in}) \\
 &\quad + \int ds ds' G_{ac}(k; \eta, s) G_{bd}(k; \eta', s') \Phi_{cd}(k; s, s'),
 \end{aligned}
 \tag{20}$$

and

$$G_{ab}(k; \eta, \eta') = [g_{ba}^{-1} - \Sigma_{ba}]^{-1}(k; \eta, \eta'),
 \tag{21}$$

where the last expression has to be interpreted in a formal sense, that is,

$$\begin{aligned}
 G_{ab}(k; \eta, \eta') &= g_{ab}(\eta - \eta') \\
 &\quad + \int ds ds' g_{ac}(\eta - s) \Sigma_{cd}(k; s, s') g_{db}(s' - \eta') + \dots
 \end{aligned}
 \tag{22}$$

Notice that, both in (20) and in (21) and everywhere else unless explicitly stated otherwise, the time integrals run from $-\infty$ to $+\infty$. However, in practice, due to the causal properties of the retarded propagators (see eq. (14)), the range of time integrations turns out to be always finite.

Eqs. (20) and (21) can be obtained either by analyzing the diagrammatic structure of the contributions at an arbitrarily high order, as in [20], or by functional methods, as in [26]. They are exact relations (*i.e.* valid at all orders in PT), and are valid both for gaussian and for non-gaussian initial conditions. Eq. (21) has been already exploited as the starting point of the derivation of the evolution equation for the propagator discussed in [22]. In the next section we will derive the evolution equation for the PS, starting from eq. (20).

In the following, we will take the initial conditions for the PS, $P_{cd}(k; \eta_{in}, \eta_{in})$, to be given by the linear PS in the growing mode, $P^0(k)u_c u_d$, which is equivalent to neglecting any nonlinear effect in the initial PS on the range of scale of interest. This

is of course exact in the $\eta_{in} \rightarrow -\infty$ limit. The linear PS in eq. (19) then becomes $P_{ab}^0(k; \eta, \eta') = u_a u_b P^0(k)$, where we have used the property of the linear propagator, $g_{ac}(\eta, \eta') u_c = u_a$, which can be checked using eqs. (14) and (16)‡.

The crucial quantities entering eqs. (20) and (21) above are the 1-particle-irreducible (1PI) functions Σ_{ab} and Φ_{ab} , where 1PI means, as usual in Feynman diagrammatic language, that the diagrams contributing to these quantities cannot be separated into two disjoint parts by cutting a single PS or propagator line. $\Sigma_{ab}(k; s, s')$ connects a dashed end at time s to a continuous one at time $s' < s$, whereas $\Phi_{ab}(k; s, s')$, connects two continuous lines at s and s' with no time ordering. The lowest order contributions to these 1PI functions are represented by the diagrams in Fig. 3, and correspond to the explicit formulae given in Appendix A.

The main focus of this paper will be on the nonlinear PS evaluated at equal times $\eta = \eta'$ (hereafter, the PS), that is,

$$P_{ab}(k; \eta) \equiv P_{ab}(k; \eta, \eta). \quad (23)$$

3. The evolution equations

In order to derive the time-evolution of $P_{ab}(k; \eta)$ we need that of $G_{ab}(k; \eta, \eta')$, which can be obtained by using the property of the linear propagator

$$\partial_\eta g_{ab}(\eta, \eta') = \delta_{ab} \delta_D(\eta - \eta') - \Omega_{ac} g_{cb}(\eta, \eta'), \quad (24)$$

in eq. (22). We get (see [22]),

$$\partial_\eta G_{ab}(k; \eta, \eta') = \delta_{ab} \delta_D(\eta - \eta') - \Omega_{ac} G_{cb}(k; \eta, \eta') + \Delta G_{ab}(k; \eta, \eta'), \quad (25)$$

where

$$\Delta G_{ab}(k; \eta, \eta') \equiv \int ds' \Sigma_{ad}(k; \eta, s') G_{db}(k; s', \eta'). \quad (26)$$

Notice that the terms containing the Dirac delta in (24) and (25) were not written in [22], because in that paper we always considered propagators at different times. Here, on the other hand, those terms are important when the propagator is inside a time integral, as in the second line of eq. (20).

Taking the η derivative of $P_{ab}(k; \eta)$ as given by (20), we get

$$\begin{aligned} \partial_\eta P_{ab}(k; \eta) &= -\Omega_{ac} P_{cb}(k; \eta) - \Omega_{bc} P_{ac}(k; \eta) \\ &\quad + \left(\Delta G_{ac}(k; \eta, \eta_{in}) G_{bd}(k; \eta, \eta_{in}) + G_{ac}(k; \eta, \eta_{in}) \Delta G_{bd}(k; \eta, \eta_{in}) \right) P_{cd}^{in}(k) \\ &\quad + \int ds ds' \Phi_{cd}(k; s, s') \left(\Delta G_{ac}(k; \eta, s) G_{bd}(k; \eta, s') + G_{ac}(k; \eta, s) \Delta G_{bd}(k; \eta, s') \right) \\ &\quad + \int ds' [\Phi_{ac}(k; \eta, s') G_{bc}(k; \eta, s') + G_{ac}(k; \eta, s') \Phi_{cb}(k; s', \eta)], \end{aligned} \quad (27)$$

which is of course still an exact equation.

‡ Remember that our fluctuations, defined in eq. (6), are constant at the linear level.

Following [22], we will approximate ΔG_{ac} as

$$\Delta G_{ac}(k; \eta, s) \simeq H_{\mathbf{a}}(k; \eta, s) G_{\mathbf{ac}}(k; \eta, s), \quad (28)$$

where

$$H_{\mathbf{a}}(k; \eta, s) \equiv \int_s^\eta ds'' \Sigma_{\mathbf{ae}}^{(1)}(k; \eta, s'') u_e,$$

with $\Sigma_{\mathbf{ad}}^{(1)}$ the 1-loop approximation to the full Σ_{ad} , see eq. (A.1), and the boldface index indicates that we are not summing over that index even if it is repeated. We will denote the solution of eq. (25) with the approximation (28) as $\bar{G}_{ab}(k; \eta, \eta')$, which we will use in (27). As it was discussed thoroughly in [22], the expression for $\bar{G}_{ab}(k; \eta, \eta')$ is exact both in the low and in the large k limits. At low k it reproduces the 1-loop propagator

$$\begin{aligned} \bar{G}_{ab}(k; \eta, \eta') &\rightarrow g_{ab}(\eta, \eta') \\ &+ \int ds ds' g_{ac}(\eta, s) \Sigma_{\mathbf{cd}}^{(1)}(k; , s, s') g_{db}(s', \eta') \quad (\text{for } k \rightarrow 0), \end{aligned} \quad (29)$$

whereas at large k it reproduces the exact result obtained by CS in [21]

$$\begin{aligned} \bar{G}_{ab}(k; \eta, \eta') &\rightarrow G_{ab}^L(k; \eta, \eta') \equiv g_{ab}(\eta - \eta') \exp \left[-k^2 \sigma_v^2 \frac{(e^\eta - e^{\eta'})^2}{2} \right], \\ &(\text{for } k \rightarrow \infty), \end{aligned} \quad (30)$$

whith σ_v^2 defined in eq. (2).

On the same spirit, we will now derive the large- k approximation of the equation for the PS. We can write the fourth line of eq. (27) as

$$\begin{aligned} &\int ds' [\Phi_{ac}(k; \eta, s') \bar{G}_{bc}(k; \eta, s') + \bar{G}_{ac}(k; \eta, s') \Phi_{cb}(k; s', \eta)] \\ &= \int ds' [\tilde{\Phi}_{ac}(k; \eta, s') \bar{G}_{bc}(k; \eta, s') + \bar{G}_{ac}(k; \eta, s') \tilde{\Phi}_{cb}(k; s', \eta)] \\ &+ \int ds' [\Delta \Phi_{ac}^L(k; \eta, s') \bar{G}_{bc}(k; \eta, s') + \bar{G}_{ac}(k; \eta, s') \Delta \Phi_{cb}^R(k; s', \eta)], \end{aligned} \quad (31)$$

where

$$\begin{aligned} \Delta \Phi_{ac}^L(k; \eta, s') &\equiv \int ds \int_{\eta_{in}}^s ds'' \Sigma_{\mathbf{ae}}^{(1)}(k; \eta, s'') u_e \bar{G}_{\mathbf{ad}}(k; \eta, s) \Phi_{dc}(k; s, s'), \\ \Delta \Phi_{cb}^R(k; s', \eta) &\equiv \int ds \int_{\eta_{in}}^s ds'' \Phi_{cd}(k; s', s) \bar{G}_{\mathbf{bd}}(k; \eta, s) \Sigma_{\mathbf{be}}^{(1)}(k; \eta, s'') u_e. \end{aligned} \quad (32)$$

The integrals of $\Sigma_{\mathbf{ae}}^{(1)}$ coming from the $\Delta \Phi$ terms ($\int_{\eta_{in}}^s ds''$) combine with those in the third line of eq. (27) ($\int_s^\eta ds''$) to give $H_{\mathbf{a}}(k; \eta, \eta_{in})$, which appears also in the second line of eq. (27). Therefore, using the exact expression in (20) the evolution equation for the PS can be written as

$$\begin{aligned} \partial_\eta P_{ab}(k; \eta) &= -\Omega_{ac} P_{cb}(k; \eta) - \Omega_{bc} P_{ac}(k; \eta) \\ &+ H_{\mathbf{a}}(k; \eta, \eta_{in}) P_{\mathbf{ab}}(k; \eta) + H_{\mathbf{b}}(k; \eta, \eta_{in}) P_{\mathbf{ab}}(k; \eta) \\ &+ \int ds [\tilde{\Phi}_{ad}(k; \eta, s) \bar{G}_{bd}(k; \eta, s) + \bar{G}_{ad}(k; \eta, s) \tilde{\Phi}_{db}(k; s, \eta)]. \end{aligned} \quad (33)$$

The solutions of the system of eqs (25) (with (28)) and (33) give the propagator and the PS valid both in the small k and in the large k limit. In the next section, we will show that, in the low k limit, it reproduces the 1-loop expressions for the PS. In sec. 6 the appropriate limit of the last line of eq. (33) in the large k limit will be computed analytically.

One can check that the (formal) solution of the system has the same form as the exact expression (20) in which the exact propagators G_{ab} have been replaced by \bar{G}_{ab} , and the full Φ_{ab} (not $\tilde{\Phi}_{ab}$!) appears.

The lowest order approximation to $\tilde{\Phi}_{ab}$, defined in (31), is just the 1-loop contribution to Φ_{ab} in Fig. 3 whose explicit expression is given in Appendix A.

4. Recovering 1-loop

As a first attack to a practical and fast solution of eq. (33), we identify the limit in which it reproduces the 1-loop result. It is obtained by using the linear expression for the PS

$$P_{ab}(k; \eta) \rightarrow P^0(k)u_a u_b, \quad (34)$$

at the second line (notice, not at the first one!) and by setting

$$\bar{G}_{ab} \rightarrow g_{ab}, \quad \tilde{\Phi}_{ab} \rightarrow \Phi_{ab}^{(1)}, \quad (35)$$

in the third line, where $\Phi_{ab}^{(1)}$ is the 1-loop approximation to $\tilde{\Phi}_{ab}$. Thus, we get

$$\begin{aligned} \partial_\eta P_{ab}^{(1)}(k; \eta) = & -\Omega_{ac} P_{cb}^{(1)}(k; \eta) - \Omega_{bc} P_{ac}^{(1)}(k; \eta) \\ & + P^0(k) \left(H_a(k; \eta, \eta_{in})u_b + H_b(k; \eta, \eta_{in})u_a \right) \\ & + \int ds \left(\Phi_{ad}^{(1)}(k; \eta, s)g_{bd}(\eta, s) + g_{ad}(\eta, s)\Phi_{db}^{(1)}(k; s, \eta) \right). \end{aligned} \quad (36)$$

The solution of the equation above exactly reproduces the 1-loop PS,

$$\begin{aligned} P_{ab}^{(1)}(k; \eta) = & P^0(k) \left[u_a u_b \right. \\ & \left. + \int ds (g_{ae}(\eta, s)u_b + g_{be}(\eta, s)u_a) H_e(k; s, \eta_{in}) \right] \\ & + \int ds ds' g_{ac}(\eta, s)g_{bd}(\eta, s')\Phi_{cd}^{(1)}(k; s, s'). \end{aligned} \quad (37)$$

as can be checked directly by taking the η -derivative of the expression above.

5. The small k limit

The approximations leading to the 1-loop result suggest the first step to take to go beyond, and to obtain a first resummation, containing infinite orders of the PT

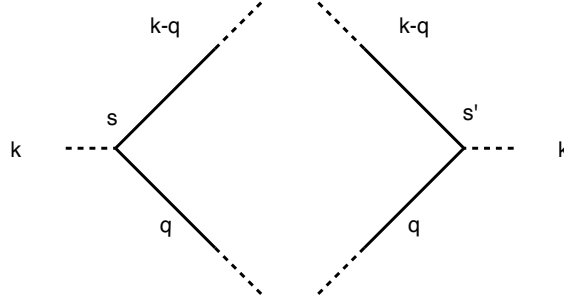


Figure 4. The 1-loop $\Phi_{ab}^{(1)}$ at the right of Fig. 3 can be obtained by gluing two mirror trees.

expansion. Indeed, by lifting the first of the three approximations used to get eq. (36) from eq. (33), namely, eq. (34), we get

$$\begin{aligned} \partial_\eta P_{ab}^{R1}(k; \eta) &= -\Omega_{ac} P_{cb}^{R1}(k; \eta) - \Omega_{bc} P_{ac}^{R1}(k; \eta) \\ &+ H_{\mathbf{a}}(k; \eta, \eta_{in}) P_{ab}^{R1}(k; \eta) + H_{\mathbf{b}}(k; \eta, \eta_{in}) P_{ab}^{R1}(k; \eta) \\ &+ \int ds [\Phi_{ad}^{(1)}(k; \eta, s) g_{bd}(\eta, s) + g_{ad}(\eta, s) \Phi_{db}^{(1)}(k; s, \eta)]. \end{aligned} \quad (38)$$

To understand what this approximation corresponds to, it is instructive to set to zero the third line of the above equation. Then, the equation can be solved exactly, to get

$$P_{ab}^{R1}(k; \eta) \Big|_{\Phi_{ab}^{(1)}=0} = \bar{G}_{ac}(k; \eta, \eta_{in}) \bar{G}_{bd}(k; \eta, \eta_{in}) u_c u_d P^0(k). \quad (39)$$

The above expression contains infinite orders in PT, and corresponds to the linear PS multiplied by two renormalized propagators. By turning $\Phi_{ab}^{(1)}$ on we are adding perturbatively the effect of mode-mode coupling.

A step further, which does not increase the computing time too much, consists in improving the second approximation, eq. (35), by using the 1-loop approximation for \bar{G}_{ab} , instead of the linear one, in the second line of eq. (33), to get

$$\begin{aligned} \partial_\eta P_{ab}^{R2}(k; \eta) &= -\Omega_{ac} P_{cb}^{R2}(k; \eta) - \Omega_{bc} P_{ac}^{R2}(k; \eta) \\ &+ H_{\mathbf{a}}(k; \eta, \eta_{in}) P_{ab}^{R2}(k; \eta) + H_{\mathbf{b}}(k; \eta, \eta_{in}) P_{ab}^{R2}(k; \eta) \\ &+ \int ds [\Phi_{ad}^{(1)}(k; \eta, s) G_{bd}^{(1)}(k; \eta, s) + G_{ad}^{(1)}(k; \eta, s) \Phi_{db}^{(1)}(k; s, \eta)], \end{aligned} \quad (40)$$

where the 1-loop propagator has been given in eq. (29).

In the following, we will present numerical results for the 1-loop approximation of eq. (37) and for the small k resummation discussed above, P_{ab}^{R2} .

6. The large k limit

In order to extend the range of validity of the approximations R1 and R2 discussed in the previous paragraph, we have to improve the approximations in eq. (35). The first

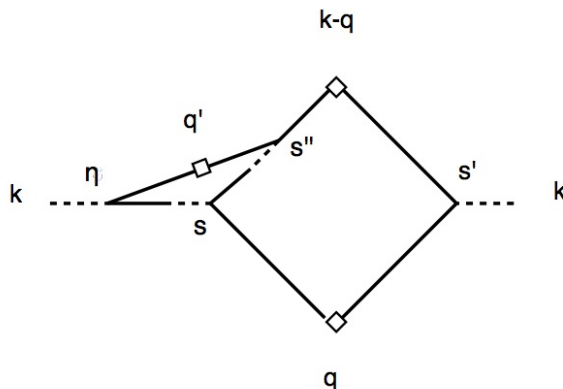


Figure 5. The lowest order contribution to Φ_{ab} not belonging to $\tilde{\Phi}_{ab}$.

one is not very problematic, as the propagator \bar{G}_{ab} can be easily computed numerically, or even analytically in the large k limit, see eq. (30).

As for the large k limit of $\tilde{\Phi}_{ab}$, we will now show that a resummation of the leading contributions to it can be performed analytically at all orders in PT, extending the CS result for the propagator [21] to the nonlinear PS.

We start from the lowest order diagram to $\tilde{\Phi}_{ab}$, namely, $\Phi_{ab}^{(1)}$, on the right of Fig. 3. The dominant contribution at large k comes from loop momentum configurations such that one of the internal PS is at a “soft” momentum $q \ll k$, and the other one is then a “hard” momentum $p = \sqrt{|\mathbf{k} - \mathbf{q}|} \simeq k$, the threshold between hard and soft being identified with the largest momentum scales contributing to the integral in (2), which, due to the large momentum damping of the Λ CDM linear PS turn out to be roughly given by $\simeq 0.18 - 0.2$ h/Mpc. For comparison, the configuration in which both internal PS’s are at a hard momentum of $O(k)$ is suppressed as $(q/k)^{3-n} \log k / \log q$, due to the $k^{n-4} \log k$ behavior of the linear PS at large momentum in Λ CDM cosmology (n is the scalar spectral index) and to the momentum dependence of the elementary vertex of eq. (7). The explicit expression of the large- k limit of $\Phi_{ab}^{(1)}$ can be obtained from eq. (A.3) or can be extracted by using the above considerations and the property of the elementary vertex of eq. (7),

$$\gamma_{abc}(\mathbf{k}, -\mathbf{k} + \mathbf{q}, -\mathbf{q}) u_c \rightarrow \delta_{ab} \frac{1}{2} \frac{\mathbf{k} \cdot \mathbf{q}}{q^2}, \quad \text{for } k \gg q, \quad (41)$$

both ways leading to

$$\Phi_{ab}^{(1)}(k; s, s') \rightarrow \Phi_{ab}^{(1),UV}(k; s, s') = k^2 \sigma_v^2 e^{s+s'} P(k) u_a u_b. \quad (42)$$

Diagrammatically, this contribution can be obtained by gluing the diagram on the left of Fig. 4 with its mirror on the right, the joints being made by the open squares representing the linear PS.

At 2-loop, the leading contributions in the large k limit are $O(k^4)$, since each of the four vertices contributes at most at $O(k)$, see eq. (41). In order to get such leading contributions we must consider all the 2-loop diagrams in which all the four vertex lie

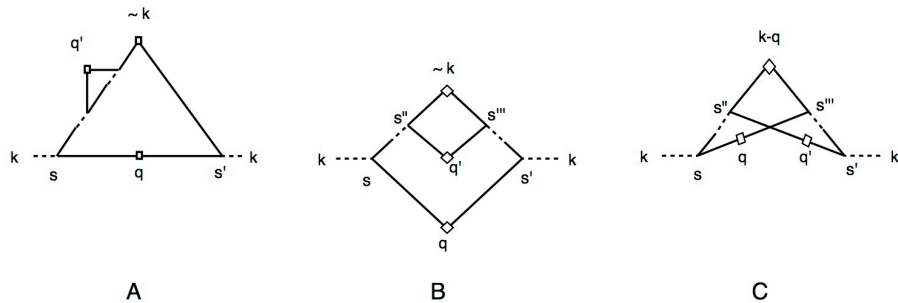


Figure 6. The 2-loop contributions to $\tilde{\Phi}_{ab}$ giving leading contributions in the large k limit.

on the hard line carrying momentum $O(k)$, and all but one PS carry soft momenta, in order to minimize the effect of the damping of the linear PS at large momentum. One of such contributions to $\Phi_{ac}(k; \eta, s')$ is represented by the diagram in Fig. 5. However, this term does not contribute to $\tilde{\Phi}_{ac}(k; \eta, s')$ since it is canceled by the $\Delta\Phi_{ac}^L(k; \eta, s')$ term in (31). On the other hand, the mirror diagram in which the soft PS corrects the vertex on the right, the one ending at the time s' , can be seen, after integration on the intermediate vertex time, s , as a renormalization of the hard propagator on the right. Therefore, the only diagrams which have to be considered at 2-loop order as large k contributions to $\tilde{\Phi}_{ab}(k; s, s')$ are those given in Fig. 6A (and its mirror) and Figs. 6B and 6C, in which two soft PS are attached in all possible ways to the hard loop line. The diagrams are qualitatively different, in a way which helps us in organizing the leading contributions in a useful way also at higher orders. Indeed, Fig. 6A is a correction to the hard propagator in the tree diagram on the left of Fig. 4 (the mirror contributions has also to be taken into account). In the large- k limit its contribution factorizes

$$-k^2 \sigma_v^2 \frac{e^{2s}}{2} \times \Phi_{ab}^{(1),UV}(k; s, s'), \quad (43)$$

where the first factor is the lowest “chain diagram” contribution to the resummed CS propagator from η_{in} to s at large- k , and we have sent $\eta_{in} \rightarrow -\infty$. The contributions in Figs. 6B and 6C, on the other hand, cannot be seen as corrections to the tree level hard propagator, but rather as PS and vertex renormalizations[§], respectively. They can be obtained by joining the two soft legs on the left tree in Fig. 7 with the right ones in the two possible ways. Using again eq. (41), and integrating in s'' and s''' from $\eta_{in} = -\infty$ to s and s' , respectively, we get the total contribution of Figs. 6B and 6C

$$2 \left(k^2 \sigma_v^2 e^{s+s'} \right)^2 P(k) u_a u_b. \quad (44)$$

At higher orders, all the leading contributions (of $O(k^{2l})$ at l -loop order) can be obtained by considering generalizations of the trees in Fig. 7, obtained by attaching

[§] More precisely, diagram 6C contains the lowest order contribution to a trilinear vertex which does not exist at tree level, namely, that with two dashed and one continuous end.

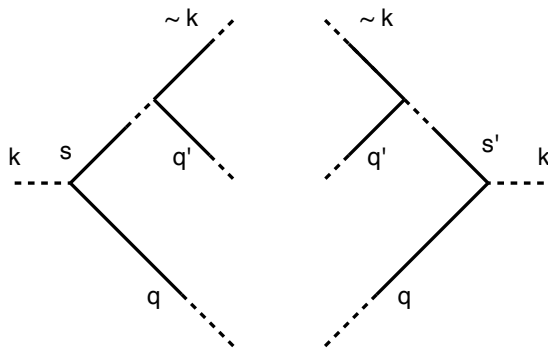


Figure 7. The two mirror trees from which the diagrams of Figs. 6B and 6C can be obtained by gluing.

new soft branches to the hard lines. In this way, each new vertex contributes at its maximum, $O(k)$, and only one PS is at the hard momentum k , the one obtained by gluing the two upper ends of the trees. Note that the two trees need not have the same number of branches, the only constraint being that the sum of all the branches be even. However, as we will discuss now, an useful separation can be made between the “intra-tree” gluings, namely, gluings between soft branches belonging to the same tree, and “inter-tree” ones. The different behavior of these two kind of gluings can be shown by considering the three diagrams in Fig. 8, which, when glued with the right tree in Fig. 7, give a 3-loop contribution to $\tilde{\Phi}_{ab}$. These diagrams can be obtained by considering a tree with four vertices, and then gluing two of the three soft branches above the vertex at time s in all the possible combinations. The remaining free branch will be eventually attached to another soft branch in the mirror tree, and will be therefore contracted with the vector u_a of eq. (16), identifying the growing mode, so that eq. (41) will apply at the vertex function to which it is attached. The three diagrams differ only in the time integrations: each one taken separately depends on the time s'' at which the unglued soft branch is attached, but the sum does not, giving the total contribution $-k^2\sigma_v^2 e^{2s}/2$, as in the first factor of eq. (43). Once these time integrals have been done, the soft branch at s'' can be attached to one of the two soft branches on the right tree, and the s'' integral can be done from $-\infty$ to s , to give

$$-k^2\sigma_v^2 \frac{e^{2s}}{2} \times 2 \left(k^2\sigma_v^2 e^{s+s'} \right)^2 P(k)u_a u_b. \quad (45)$$

Summing together eqs. (42) to (45), we get

$$\left(1 - k^2\sigma_v^2 \frac{e^{2s}}{2} \right) \times \left[k^2\sigma_v^2 e^{s+s'} + 2 \left(k^2\sigma_v^2 e^{s+s'} \right)^2 \right] P(k)u_a u_b, \quad (46)$$

from which we see that the 1-loop correction to the hard propagator (first factor) factorizes from the contribution given by the gluing of the two mirror trees with equal numbers of lines of Figs. 4 and 7.

Therefore, we can perform the resummation of the two hard propagator lines independently and concentrate on the gluing: in other words, we can consider trees

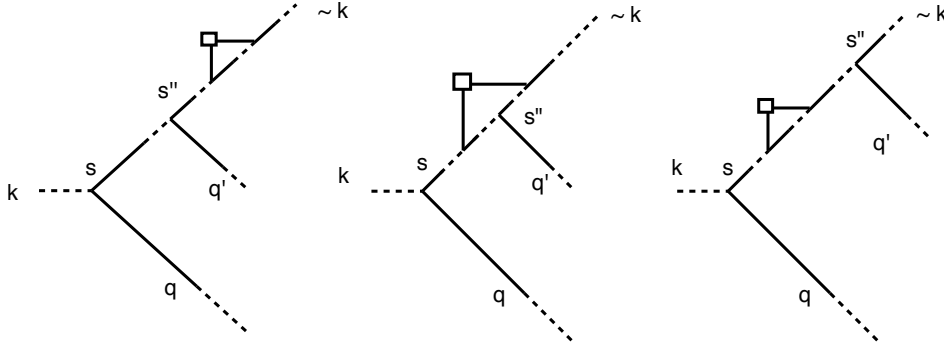


Figure 8. In the large k limit, the s'' dependence from each of the time integrations cancels in the sum of the three contributions.

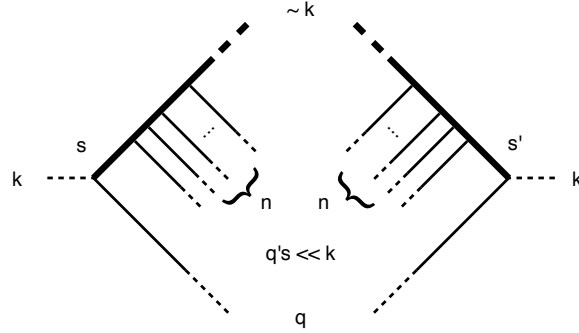


Figure 9. Once the hard branches (thick lines) have been resummed to give the CS form of eq. (30), all the contributions to $\tilde{\Phi}_{ab}$ can be obtained by gluing two (renormalized) mirror trees.

as in Fig. 9, where the thick propagator lines correspond to the large k propagators of eq. (30), n soft lines are attached to each of them, and, together with the soft line attached at the vertex in s , each of the $n + 1$ soft legs from one tree are glued with the $n + 1$ ones from the mirror tree in all possible combinations. Taking into account that the time integrations on the n soft branch insertions on the left and on the right give a $e^{n(s+s')}/(n!)^2$ factor and summing over the $(n + 1)!$ possible gluings, the contribution of all possible diagrams obtained from Fig. 9 reads

$$e^{-\frac{k^2\sigma_v^2}{2}(e^{2s}+e^{2s'})} \frac{n+1}{n!} \left(k^2\sigma_v^2 e^{s+s'}\right)^{n+1} P(k)u_a u_b, \quad (47)$$

which can be summed from $n = 0$ to ∞ , to give the large- k limit of $\tilde{\Phi}_{ab}(k; s, s')$,

$$\begin{aligned} \tilde{\Phi}_{ab}(k; s, s') &\rightarrow e^{-\frac{k^2\sigma_v^2}{2}(e^s-e^{s'})^2} F[k^2\sigma_v^2 e^{s+s'}]P(k)u_a u_b, \\ \text{where } F[x] &= x(1+x). \end{aligned} \quad (48)$$

Remarkably, the expression above, multiplied by the large k expression for the propagator, eq. (30), as in the last line of eq. (33) can be integrated analytically in s to

give

$$\int ds [\tilde{\Phi}_{ad}(k; \eta, s) G_{bd}^L(k; \eta, s) + G_{ad}^L(k; \eta, s) \tilde{\Phi}_{ab}(k; s, \eta)] \rightarrow u_a u_b P^0(k) [y^2(e^{-y^2} - 1) + \sqrt{\pi} y(1 + y^2) \text{Erf}(y)], \quad \text{where } y \equiv e^\eta k \sigma_v, \quad (49)$$

and ‘‘Erf’’ is the error function, $\text{Erf}(y) \equiv 2\pi^{-1/2} \int_0^y dt e^{-t^2}$. We reiterate that the above expression is valid in the large momentum limit, which is more precisely given by $y \gg 1$. In this limit, it goes as $P^0(k) \sqrt{\pi} y^3 (1 - 1/y\sqrt{\pi} + 1/y^2)$. Considering that H_a and H_b in eq. (33), in the same limit, go as $-y^2$, we realize that in the large- y limit the differential equation in (33) has an attractor solution, given by the simple formula

$$P_{ab}(k; \eta) \rightarrow \frac{\sqrt{\pi}}{2} y \left(1 - \frac{1}{y\sqrt{\pi}} + \frac{1}{y^2} \right) u_a u_b P^0(k), \quad \text{for } y \gg 1, \quad (50)$$

which shows that the effect of nonlinearities (including mode-mode coupling) on the PS in the extreme large y limit is just a multiplicative renormalization of the *linear* PS!

7. Matching small and large k

In the previous two sections we have obtained the limiting expressions for the mode-mode coupling term in the evolution equation, the third line of eq. (33). In the small k limit, it is given by the 1-loop expression in eq. (38), or by its improved version, eq. (40), whereas, at large k , it is given by eq. (49). In order to cover also the intermediate k range we should interpolate between these limiting behaviors. As a first step, we notice that, in the range of scales that we will consider, namely $k < O(1 \text{ h/Mpc})$, the 1-loop function $\Phi_{ab}^{(1)}(k; s, s')$, particularly the $a = b = 1$ component, has not yet converged to its UV limit $\Phi_{ab}^{(1), \text{UV}}(k; s, s')$ of eq. (42), see Fig. 10. This fact has an impact on the contributions coming from all the diagrams considered in our resummation that can be obtained as corrections of $\Phi_{ab}^{(1)}(k; s, s')$, namely, at 2-loops, from the contributions of Figs. 6A and 6B, but not 6C. These contributions can be then reconsidered at any order, by identifying those gluings of the trees in Fig. 9 where the two lower lines carrying momentum q are joined together, and restoring the full k -dependence of $\Phi_{ab}^{(1)}$ for them. This procedure leads to the improved version of eq. (48)

$$\tilde{\Phi}_{ab}(k; s, s') \rightarrow e^{-\frac{k^2 \sigma_v^2}{2} (e^s - e^{s'})^2} \left[\Phi_{ab}^{(1)}(k; s, s') + \left(k^2 \sigma_v^2 e^{s+s'} \right)^2 P(k) u_a u_b \right] \quad (51)$$

that is the correct high momentum limit for $\tilde{\Phi}_{ab}$, valid also at not extreme values for k (or y).

At small k , the above expression explicitly goes to $\Phi_{ab}^{(1)}$. The $O(k^4 P^0(k))$ term inside parentheses is the large k limit of the 2-loop diagram in 6C. At low k this diagram has a different behavior (it goes as k^4 times a constant), and moreover it becomes degenerate with other 2-loop contributions not included in this resummation. The cleanest way to take these terms into account would be to subtract the large k 2-loop contribution and

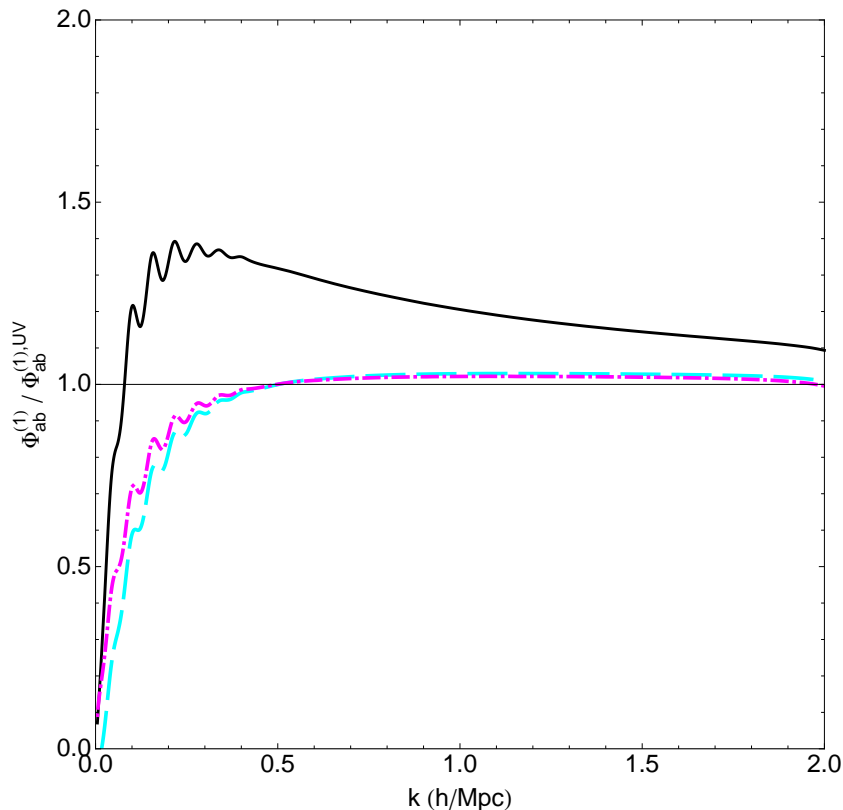


Figure 10. The redshift-independent ratio between the components of $\Phi_{ab}^{(1)}$ in eq. (A.3), and their large k limit, eq. (42). The black solid line is $\Phi_{11}^{(1)}$, the cyan-dashed line is $\Phi_{12}^{(1)}$, and the magenta dash-dotted one is $\Phi_{22}^{(1)}$.

to add the full 2-loop one. However, in order to be consistent with the treatment for the propagator, which matches 1-loop (not 2-loop) PT at $k \rightarrow 0$, and to avoid the numerical evaluation of 2-loop integrals, we simply suppress the $O(k^4 P(k))$ terms from eq. (51) at small k by multiplying the second term inside the parenthesis by a filter function of the form

$$F(k) = \frac{(k/\bar{k})^4}{1 + (k/\bar{k})^4}, \quad (52)$$

see also eq. (B.7), where the power 4 ensures a rapid enough switch-off of the filter at low k . We choose $\bar{k} = 0.2$ h/Mpc for the threshold value, since for larger momenta the $O(k^4 P(k))$ term in eq. (51) starts to dominate over $\Phi_{ab}^{(1)}$. Alternatively, we can take \bar{k} as a parameter to be marginalized in a fit to real data. In any case, as we will see in next section, see Fig. 13, the filter becomes irrelevant at large k and for redshifts $\gtrsim 1$.

As for the propagator \bar{G}_{ab} entering the third line of eq. (33) we have already mentioned that it provides an interpolation between the 1-loop propagator at $k \rightarrow 0$ and the large k resummed one of eq. (30) [22]. Therefore, we could, in principle, solve eq. (25) for different initial and final times, and then use these solutions in eq. (33). However, a faster procedure is to use analytic approximations to the full propagator, having the same limiting behaviors as \bar{G}_{ab} , since in this case, the integrations in s can

be done analytically. One such expression, which was proved in [40] to fit very well with N-body simulations is the following

$$G_{ab}^{(BCS)}(k, \eta, \eta') = \left[G_{ab}^{(1)}(k; \eta, \eta') + k^2 \sigma_v^2 \frac{(e^\eta - e^{\eta'})^2}{2} \Theta(\eta - \eta') \right] \exp \left[-k^2 \sigma_v^2 \frac{(e^\eta - e^{\eta'})^2}{2} \right], \quad (53)$$

where, at large k , the second term in parentheses exactly cancels $\delta G_{ab} = G_{ab}^{(1)} - g_{ab}$, and gives $G_{ab}^{(BCS)} \rightarrow G_{ab}^L$, while, at small k , $G_{ab}^{(BCS)} \rightarrow G_{ab}^{(1)}(1 + O(k^4))$.

In our numerical analysis, we tested the difference between using the propagator \bar{G}_{ab} , $G_{ab}^{(BCS)}$, or simply G_{ab}^L in the third line of eq. (33), finding basically no difference at the percent level in the full range of scales considered. Since using G_{ab}^L turns out to be much faster, we recommend using it in numerical implementations of the scheme presented in this paper. Explicit formulae are given in Appendix B.

8. Numerical results: comparison with N-body simulations

The aim of this section is to test numerically the goodness of our approach. We compared the nonlinear PS predictions against the data coming from high accuracy N-body simulations designed to predict the nonlinear PS at the percent accuracy around the BAO range of scales. The initial linear PS for the simulations we considered was obtained from the CAMB public code [43] and any primordial non-Gaussianity was neglected. Accordingly, we solved our evolution equations taking the initial PS from CAMB at $z_{in} = 100$, where the gravitational clustering is fully linear on the scales of interest.

We provide plots of the comparison between our approach and the N-body simulations presented by Sato and Matsubara in [35]. They considered a Λ CDM cosmology with the following parameters: $\Omega_m = 0.265$, $\Omega_b h^2 = 0.0226$, $h = 0.71$, $n = 0.963$ and $\sigma_8 = 0.8$. In order to check the possible dependence of our results on the cosmology or on the N-body simulations, we also compared our results with the independent set of simulations produced by Carlson, White and Padmanabhan in [44] for a different Λ CDM cosmology, and with the results from the cosmic Coyote emulator [13, 41, 42]. The latter is an interpolator built from a suite of many different N-body simulations which provides nonlinear PS's for different cosmological parameters chosen inside a certain range and for redshifts $z \leq 1$. In all these cases our comparison tests worked at the same quality level.

In Fig. 11 we plot the nonlinear PS computed in different approximations, divided by the smooth linear PS given in [36]. The blue dashed line corresponds to the small k approximation of eq. (40), while the red solid line is obtained by using eq. (51) at the third line of (33), with the form (30) for the propagator and the filter function of eq. (52). Explicit formulae are given in Appendix B. The results obtained in linear PT (grey dash-dotted) and 1-loop PT (been dotted) are also shown. Relative differences

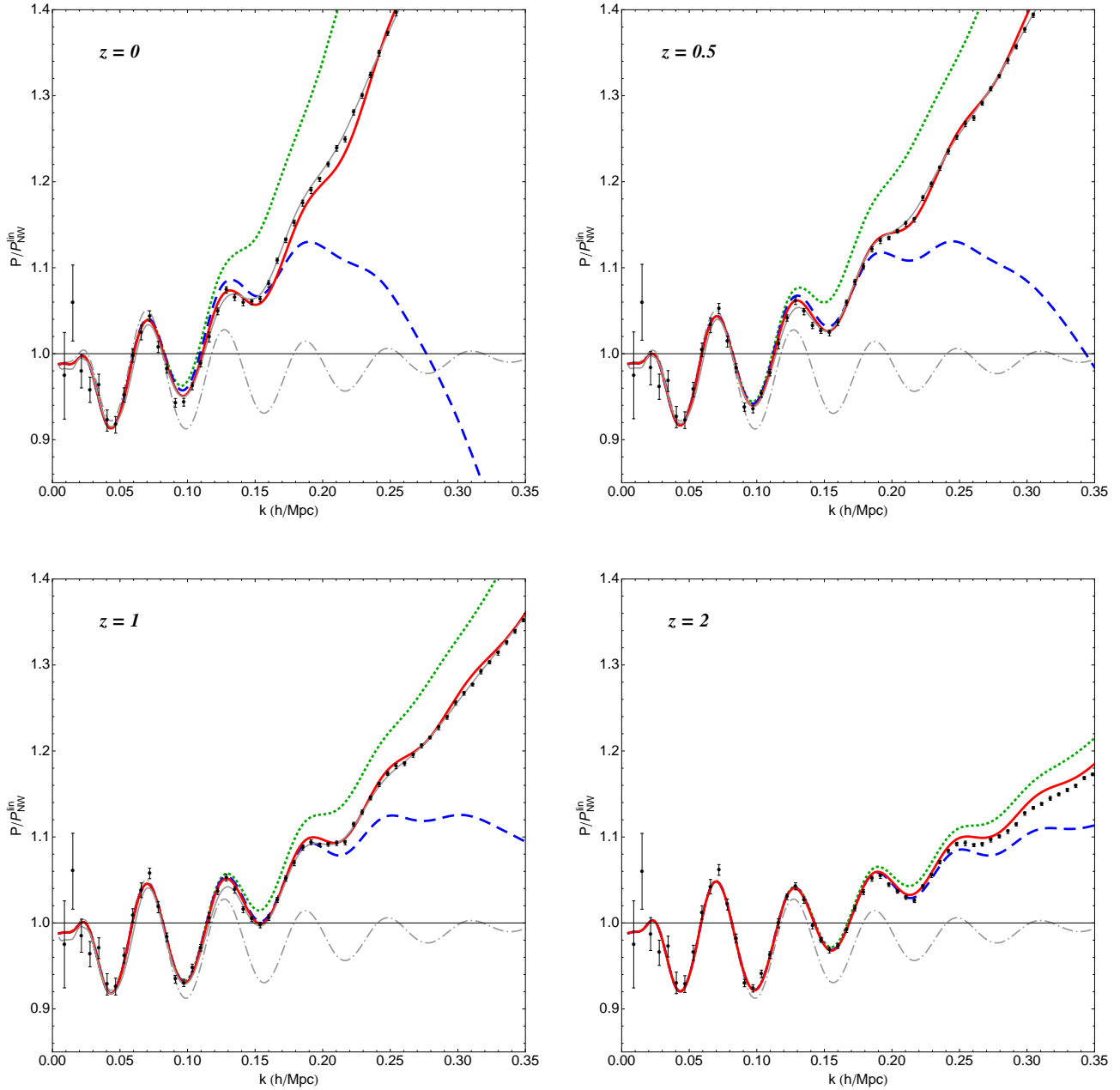


Figure 11. PS's normalized to the no-wiggle PS of [36] at different redshifts. The color code is the following: the grey dash-dotted line is linear PT, the green dotted line is 1-loop PT, the blue dashed line corresponds to the solution of the evolution equation in the small k approximation “R2” of eq. (40), the red solid line is the solution of the evolution equation (33) with the resummed Φ_{ab} given in eq. (51) and the power-law filter function of eq. (52) with $\bar{k} = 0.2$ h/Mpc, and dots with error-bars are the N-body results of Sato and Matsubara [35]. Also shown (thin grey line) is the output of the Coyote interpolator of refs. [13, 41, 42].

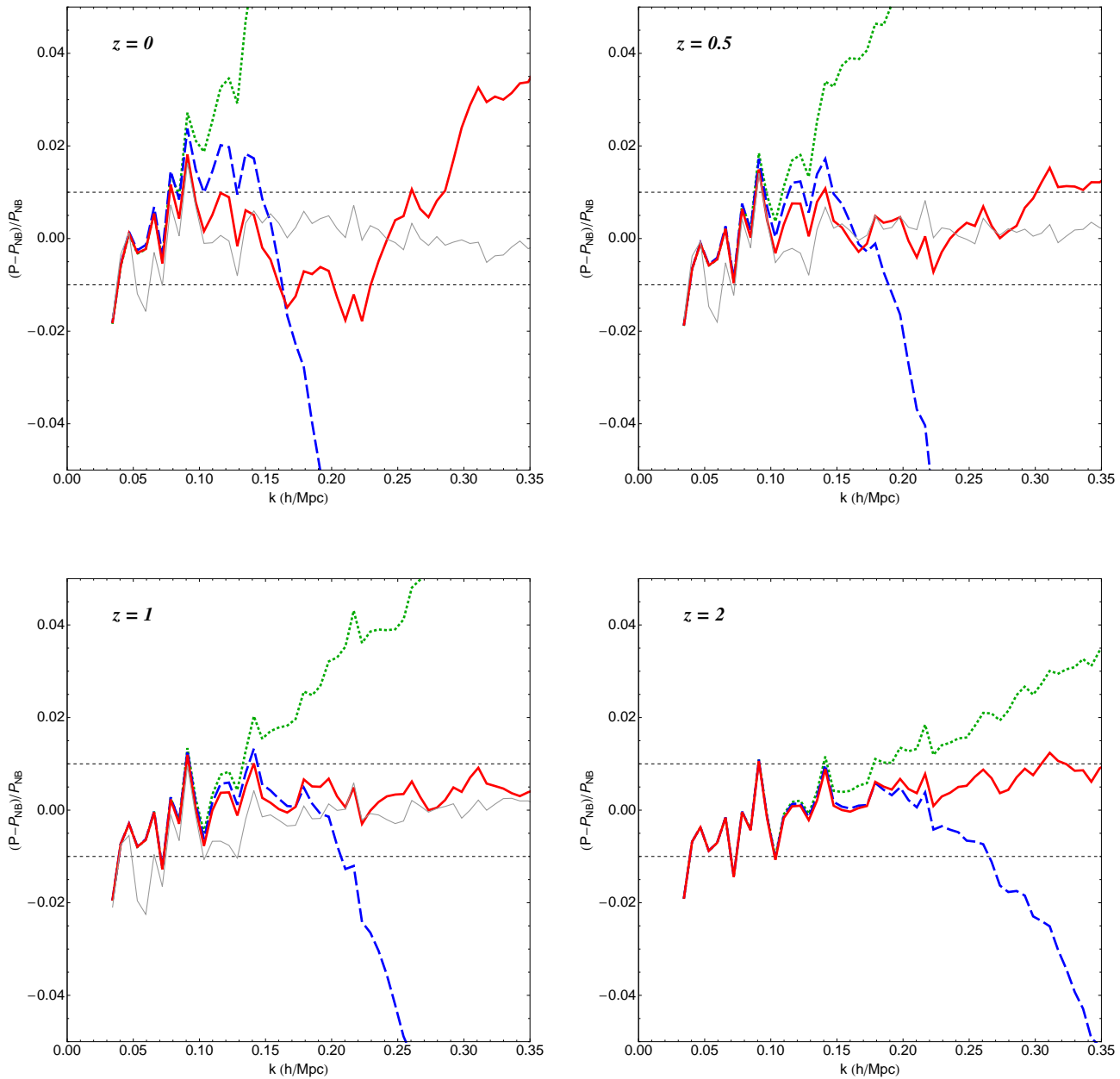


Figure 12. The relative difference between various approximations discussed in the text and the N-body simulations of Sato and Matsubara [35]. Same color-code as in Fig. 11. The thin grey line is the comparison with the output of the Coyote interpolator.

with respect to the N-body results are given in Fig. 12 with the same color-code.

We notice that our evolution equation (33), in the small k limit of eq. (40), *i.e.* with no-resummation of the contributions to $\tilde{\Phi}_{ab}$ beyond 1-loop order, is able to reproduce the nonlinear PS at the percent level in the BAO range. There are a couple of outlier points in the linear region $k < 0.1$ h/Mpc which can be ascribed to a fluctuation in the N-body simulations of [35] from a comparison with the Coyote emulator (thin grey line in Fig. 11, 12) and with the 1-loop approximations, which works well in this region.

Concerning the resummed and interpolated solution, *i.e.* the red line, we see that it performs at the 1% level in the BAO region at any redshift, including $z = 0$, where, due to the larger amount of nonlinearity, the last peak is at about 0.15 h/Mpc. At redshifts $z \geq 0.5$ it performs as the Coyote interpolator up to $k \simeq 0.35$ h/Mpc, namely, still in agreement with the N-body results of [35] at the 1% level.

In Fig. 13, we plot, in an extended k range, the results obtained as in the red line of Fig. 11 with (thick red) and without (thin red) the filter function of eq. (52). We see that, as expected, the effect of the filter vanishes at large k (where the filter goes to unity) and at increasing redshift, where the difference between the full 2-loop contributions and their large k expression contained in eq. (51) becomes less relevant. We also plot (thick black dashed line) the result obtained by using the large k expression for $\Phi_{ab}^{(1)}$, eq. (42), in eq. (51), namely eq. (33) where we use eq. (49) for the third line. We also show the analytic expression for the attractor solution found in eq. (50) (thin black dashed line).

The comparison with the nonlinear PS from the N-body simulations at large k is given in Fig. (14). In order to gauge the performance of the N-body results at large k , Sato and Matsubara performed runs with two different volumes, a large one ($L_{box} = 1000$ Mpc/h) and a small one ($L_{box} = 500$ Mpc/h), which we plot with black and blue points, respectively. We notice that the two sets of data are practically overlapped for $z < 1$, where we also checked that they agree with the Coyote emulator, but diverge significantly at $z \geq 2$ for $k \gtrsim 0.8$ h/Mpc. These transient effects therefore prevent us from considering the comparison for higher redshifts and scales, however, the trend from $z = 0$ up to $z = 2$ clearly shows a progressive improvement, as it should. Quantitatively, at $z = 1$ we measure an agreement at the 1% level between our results and the N-body simulations up to $k = 0.8$ h/Mpc and at 2% on the same range of scales for $z = 0.5$.

9. Discussion and conclusions

The scheme discussed in this paper presents three main advantages with respect to alternative approaches to the nonlinear PS in the $k \lesssim 1$ h/Mpc scale, including N-body simulations: the accuracy (already discussed in the previous section), the computational time, and the range of cosmologies that can be dealt with. The computational time is the same as that required by a standard PT computation at 1-loop. Indeed, concerning momentum integrations, to obtain the three independent components of the PS, one needs to perform two one-dimensional integrals, eqs. (B.1) and (B.2), and the three two-dimensional ones of eq. (A.3). Exactly the same integrals enter the 1-loop expression for the PS, eq. (37). In addition, the solution of our evolution equation requires only one more integration in time, or better, in η , which however takes a time of the order of a second. Therefore, any point in k takes at most a few seconds to be evaluated.

The extension from Λ CDM cosmology to more general ones is also greatly eased in this approach. In principle, all the cosmologies in which the fluid equations of eq. 3 are modified only in the linear terms, can be taken into account by a modification of

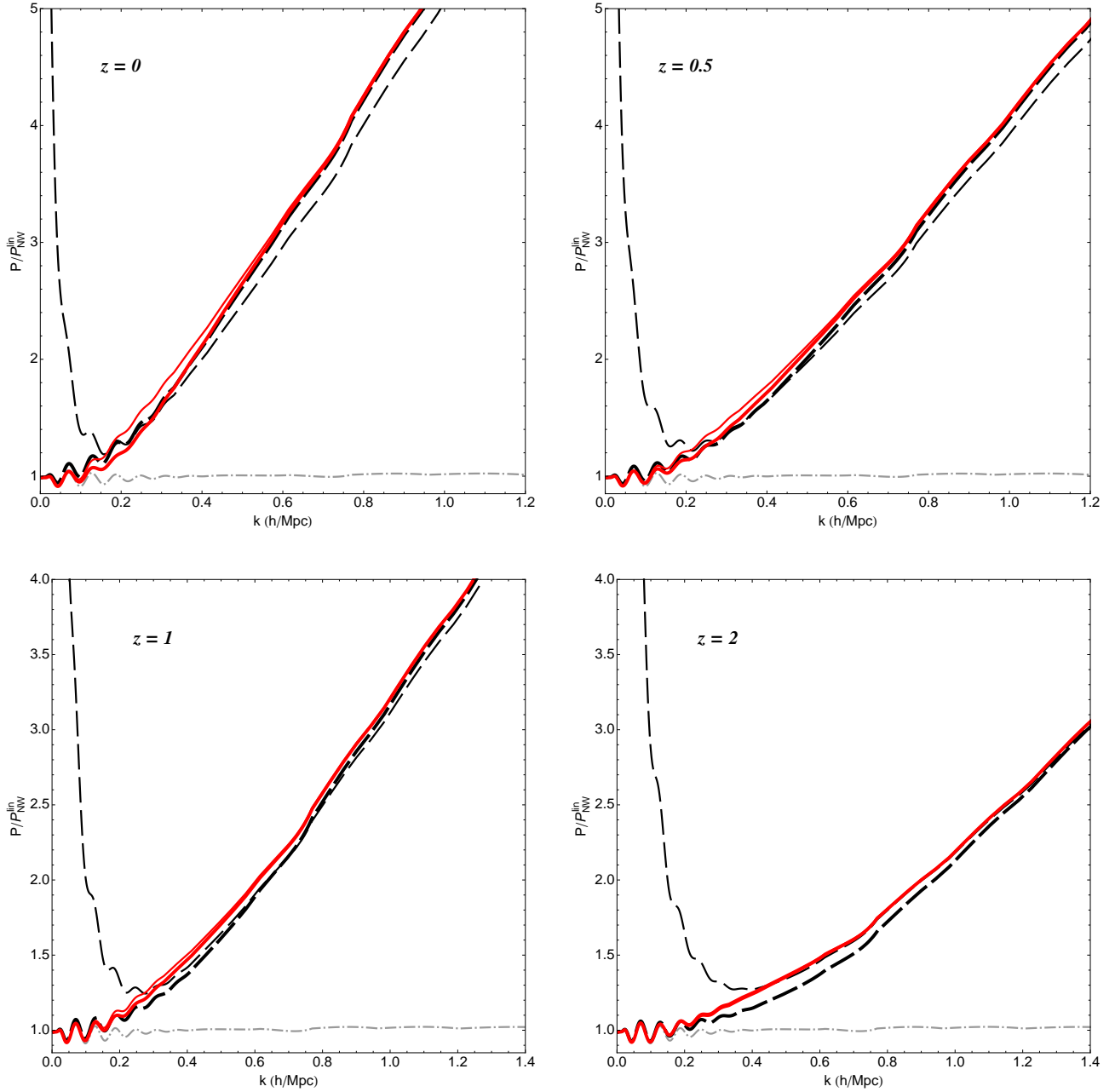


Figure 13. The PS at large k from the evolution equation in various approximations for the mode-mode coupling part in the third line of eq. (33) and at different redshifts. The thick black dashed line corresponds to using eq. (49), the thin red solid line to the improved $\tilde{\Phi}_{ab}$ of eq. (51), and the thick red solid line to using eq. (51) with the power-law filter function of eq. (52) with $\bar{k} = 0.2$ h/Mpc (see Appendix B for explicit formulae). Also shown are the large y attractor solution of eq. (50) (thin black dashed line), and linear PT (grey dash-dotted line).

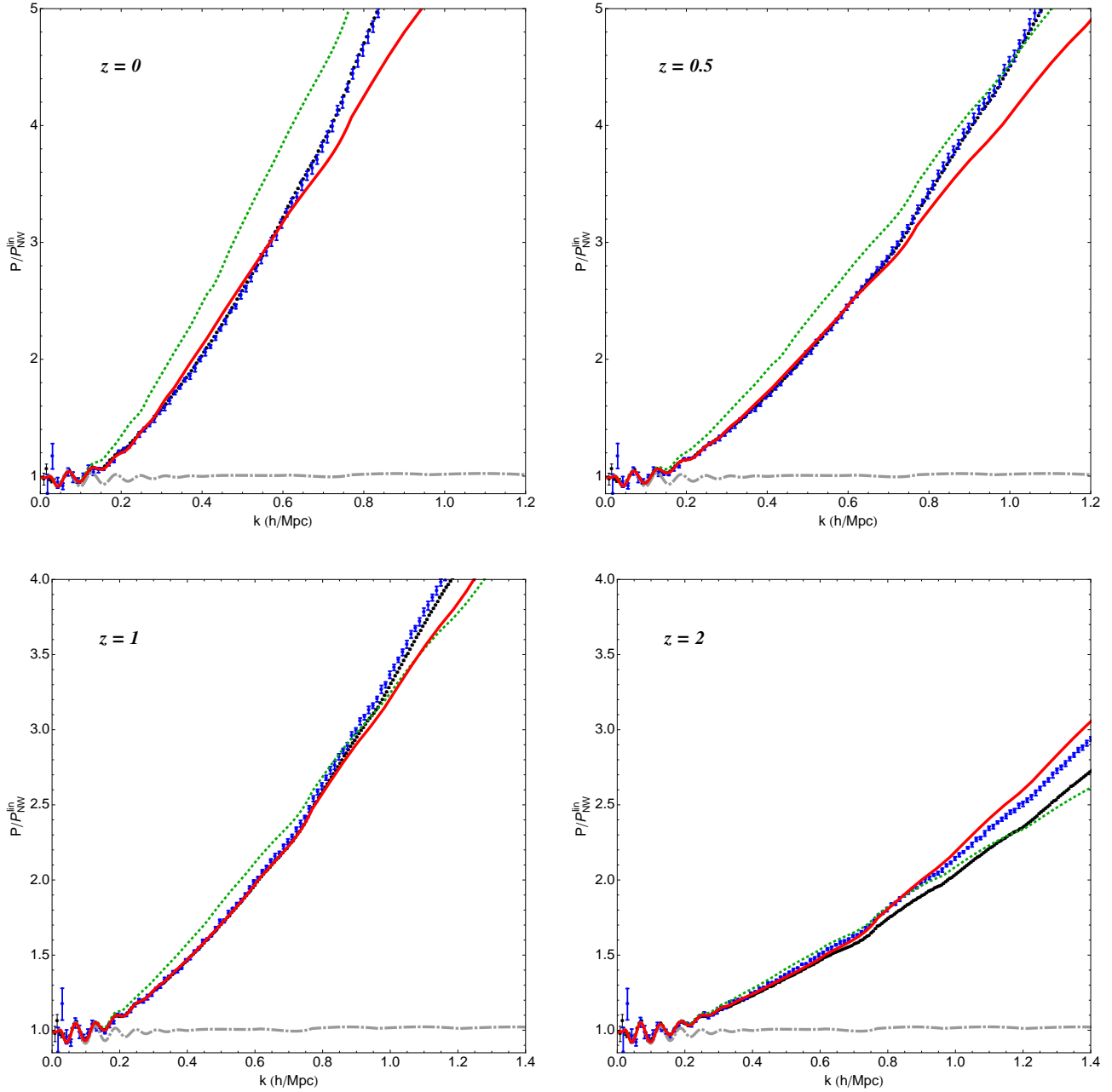


Figure 14. Comparison between the evolution equation discussed in this paper (red solid line, see Appendix B for explicit formulae), and the N-body simulations of Sato and Matsubara [35]: black dots are for the large volume simulation ($L = 1000 \text{ Mpc}/h$), blue ones for the small volume one ($L = 500 \text{ Mpc}/h$). Also shown are linear PT (grey dash-dotted line) and 1-loop PT (green dotted line).

the Ω matrices in (9), as it was discussed in [14]. Cosmologies of this type include, for instance, those with massive neutrinos [45, 46, 47], modifications of gravity of the scalar-tensor/f(R) type [48], or Dark Energy models with a non-relativistic sound speed [18]. Non-gaussian initial conditions can also be taken into account by the inclusion of new vertices in the diagrammatic rules of Fig. 2 and their impact on the propagator and on the PS can be analyzed [49, 50].

Evolution equations for the nonlinear PS have been proposed also before [51, 27, 14, 52]. The main step forward provided by the present analysis is, besides the computational speed, the correct treatment of the large k limit, in particular for the mode-mode coupling term. Indeed, while the gaussian damping of the contribution proportional to the linear PS, namely the first term in eq. (20), is reproduced satisfactorily well by most resummed PT methods, the remaining part, that containing the mode-mixing function Φ_{ab} is usually included only at lowest order in PT, adding at most a few corrections. As a result, the improvement of these methods over the 1-loop results was not able to go beyond the BAO scale, as it was discussed in detail for the Time Renormalization Group approach of ref. [14] in [53, 32].

A different strategy to resum PT corrections at all orders is provided by the approach of [24]. In this context, it was shown that the exact CS resummation for the propagator holds also for the larger class of multipoint propagators. The nonlinear PS can be expressed as an infinite sum over squares of multi-point propagators, however the kinematical regime for which the exact resummation was proved is not the one relevant to the calculation of the PS at large k , namely, the one in which only one internal PS is at large k , the other ones being soft.

The approach presented in this paper suffers from an intrinsic physical limitation, namely, the neglect of velocity dispersion and all higher order moments of the particle distribution function, which are at the basis of the derivation of eqs. (3) from the Vlasov equation. This “single stream approximation” is known to hold at large scales and high redshifts, but it was estimated to fail at the percent level in the BAO range at $z \rightarrow 0$ [37, 38]. The comparison of sect. 8 between our results and N-body simulations exhibits the same trend. In other words, it is consistent with the hypothesis that our approach captures all the relevant physics contained in the fluid equations (3). The access to the multi-stream regime is precluded by construction to all forms of (improved) PT, including this one. A way to incorporate such effects in semi-analytical methods was recently proposed in [39], in which the feeding of the multi stream at small scales on the more perturbative intermediate scales was described in terms of effective source terms. The inclusion of such effects in the present approach will be studied elsewhere.

For the time being, the increase of the maximum k at which the nonlinear PS can be computed reliably, provided by our approach, opens the way to interesting cosmological applications, allowing a tighter extraction of cosmological parameters from the LSS relevant for topics such as the measurement of the acoustic scale from BAO’s, the limit on the neutrino mass scale, and possibly, cosmic shear.

Acknowledgments

We thank M. Sato and T. Matsubara as well as M. White and J. Carlson for providing the simulations data. We thank M. Crocce for useful discussions. SA would like to acknowledge Institut de Ciències de l'Espai (IEEC/ICE), Barcelona, Spain, for hospitality, “Fondazione Angelo Della Riccia” and “Fondazione Ing. Aldo Gini” for financial support. MP acknowledges partial support from the European Union FP7 ITN INVISIBLES (Marie Curie Actions, PITN- GA-2011- 289442).

Appendix A.

In this appendix we will give the explicit expressions of the 1PI functions $\Sigma_{ab}^{(1)}(k; \eta, \eta')$ and $\Phi_{ab}^{(1)}(k; \eta, \eta')$ computed at 1-loop. The general expression for $\Sigma_{ab}^{(1)}(k; \eta, \eta')$ is given by

$$\Sigma_{ab}^{(1)}(k; \eta, \eta') = 4e^{\eta+\eta'} \int d^3q \gamma_{acd}(\mathbf{k}, -\mathbf{q}, \mathbf{q} - \mathbf{k}) u_c P^0(q) u_e \gamma_{feb}(\mathbf{k} - \mathbf{q}, \mathbf{q}, -\mathbf{k}) g_{df}(\eta, \eta'),$$

which, using the expressions for the vertices and the linear propagator in eqs. (7), (14), and performing the angular integration, gives

$$\begin{aligned} \Sigma_{11}^{(1)}(k; \eta, \eta') &= -e^{-3/2\eta+\eta'} \frac{k^3 \pi}{15} \int dr P^0(kr) \left[3e^{5/2\eta}(1-3r^2) \right. \\ &\quad \left. + e^{5/2\eta'}(17+9r^2) + \frac{9}{2r} (e^{5/2\eta} - e^{5/2\eta'}) (r^2-1)^2 \log \left| \frac{1+r}{1-r} \right| \right], \\ \Sigma_{12}^{(1)}(k; \eta, \eta') &= -e^{-3/2\eta+\eta'} \frac{k^3 \pi}{15} (e^{5/2\eta} - e^{5/2\eta'}) \int dr P^0(kr) \left[8 - 15r^2 + 9r^4 \right. \\ &\quad \left. - \frac{9r}{2} (r^2-1)^2 \log \left| \frac{1+r}{1-r} \right| \right], \\ \Sigma_{21}^{(1)}(k; \eta, \eta') &= -e^{-3/2\eta+\eta'} \frac{3k^3 \pi}{5} (e^{5/2\eta} - e^{5/2\eta'}) \int dr P^0(kr) \left[\frac{1}{r^2} (3r^2-1) \right. \\ &\quad \left. + \frac{1}{2r^3} (r^2-1)^2 \log \left| \frac{1+r}{1-r} \right| \right], \\ \Sigma_{22}^{(1)}(k; \eta, \eta') &= -e^{-3/2\eta+\eta'} \frac{k^3 \pi}{15} \int dr P^0(kr) \left[3e^{5/2\eta'}(1-3r^2) + e^{5/2\eta}(17+9r^2) \right. \\ &\quad \left. - (e^{5/2\eta} - e^{5/2\eta'}) \frac{9}{2r} (r^2-1)^2 \log \left| \frac{1+r}{1-r} \right| \right]. \end{aligned} \quad (\text{A.1})$$

The general expression for the 1-loop contribution to $\Phi_{ab}^{(1)}(k; \eta, \eta')$ is

$$\begin{aligned} \Phi_{ab}^{(1)}(k; \eta, \eta') &= 2e^{\eta+\eta'} \int d^3q \gamma_{acd}(\mathbf{k}, -\mathbf{q}, -\mathbf{p}) u_c P^0(q) u_e u_d P^0(p) u_f \gamma_{bef}(-\mathbf{k}, \mathbf{q}, \mathbf{p}), \end{aligned} \quad (\text{A.2})$$

with $\mathbf{p} = \mathbf{k} - \mathbf{q}$, which gives the following expressions for the individual components,

$$\begin{aligned}
 \Phi_{11}^{(1)}(k; \eta, \eta') &= e^{\eta+\eta'} \frac{\pi}{4k} \int_0^\infty dq \int_{|k-q|}^{k+q} dp \frac{[k^2(p^2 + q^2) - (p^2 - q^2)^2]^2}{p^3 q^3} P^0(q) P^0(p), \\
 \Phi_{12}^{(1)}(k; \eta, \eta') &= e^{\eta+\eta'} \frac{k\pi}{4} \int_0^\infty dq \int_{|k-q|}^{k+q} dp \frac{(k^2 - p^2 - q^2) [k^2(p^2 + q^2) - (p^2 - q^2)^2]}{p^3 q^3} P^0(q) P^0(p), \\
 \Phi_{21}^{(1)}(k; \eta, \eta') &= \Phi_{12}^{(1)}(k; \eta, \eta'), \\
 \Phi_{22}^{(1)}(k; \eta, \eta') &= e^{\eta+\eta'} \frac{k^3 \pi}{4} \int_0^\infty dq \int_{|k-q|}^{k+q} dp \frac{(k^2 - p^2 - q^2)^2}{p^3 q^3} P^0(q) P^0(p). \quad (\text{A.3})
 \end{aligned}$$

Appendix B.

In this appendix we will give the explicit formulae to be inserted in the evolution equation for the nonlinear PS, eq. (33). The first line contains the matrix Ω_{ab} , defined in eq. (9). At the second line, the two functions $H_1(k; \eta, -\infty)$ and $H_2(k; \eta, -\infty)$ appear, which are given explicitly by

$$\begin{aligned}
 H_1(k; \eta, -\infty) &= \int_{-\infty}^\eta ds \Sigma_{1b}^{(1)}(k; \eta, s) u_b = \\
 &= e^{2\eta} \frac{k^3 \pi}{21} \int dr \left[19 - 24r^2 + 9r^4 - \frac{9}{2r} (r^2 - 1)^3 \log \left| \frac{1+r}{1-r} \right| \right] P^0(kr), \quad (\text{B.1})
 \end{aligned}$$

$$\begin{aligned}
 H_2(k; \eta, -\infty) &= \int_{-\infty}^\eta ds \Sigma_{2b}^{(1)}(k; \eta, s) u_b = \\
 &= e^{2\eta} \frac{k^3 \pi}{21} \int dr \left[-\frac{9}{r^2} + 52 + 9r^2 - \frac{9}{2r^3} (r^2 - 1)^3 \log \left| \frac{1+r}{1-r} \right| \right] P^0(kr). \quad (\text{B.2})
 \end{aligned}$$

As we have discussed in the text, the third line of eq. (33) is well approximated by using the small scale expression for $\tilde{\Phi}_{ab}$ given in eq. (51), and the small scale analytic expression for the propagator, G_{ab}^L , instead of the solution of eq. (25) with eq. (28), namely, \bar{G}_{ab} . The time integration can then be done analytically, to get.

$$\begin{aligned}
 &\int ds [\tilde{\Phi}_{ad}(k; \eta, s) G_{bd}^L(k; \eta, s) + \bar{G}_{ad}^L(k; \eta, s) \tilde{\Phi}_{db}(k; s, \eta)] \\
 &= \tilde{\Phi} G_{ab}^A(k; \eta) + \tilde{\Phi} G_{ab}^B(k; \eta), \quad (\text{B.3})
 \end{aligned}$$

where

$$\tilde{\Phi} G_{11}^A(k; \eta) = \frac{\sqrt{\pi} \text{Erf}(y)}{y} \left(\frac{3\Phi_{11}^{(1)}(k; \eta, \eta)}{5} + \frac{2\Phi_{12}^{(1)}(k; \eta, \eta)}{5} \right)$$

$$\begin{aligned}
 & + \frac{8}{525} \mathcal{B}(y^2) (\Phi_{11}^{(1)}(k; \eta, \eta) - \Phi_{12}^{(1)}(k; \eta, \eta)), \\
 \tilde{\Phi}G_{12}^A(k; \eta) &= \frac{\sqrt{\pi} \operatorname{Erf}(y)}{y} \left(\frac{3\Phi_{11}^{(1)}(k; \eta, \eta)}{10} + \frac{\Phi_{12}^{(1)}(k; \eta, \eta)}{2} + \frac{\Phi_{22}^{(1)}(k; \eta, \eta)}{5} \right) \\
 & - \frac{2}{525} \mathcal{B}(y^2) (3\Phi_{11}^{(1)}(k; \eta, \eta) - 5\Phi_{12}^{(1)}(k; \eta, \eta) + 2\Phi_{22}^{(1)}(k; \eta, \eta)), \\
 \tilde{\Phi}G_{21}^A(k; \eta) &= \tilde{\Phi}G_{12}^A(k; \eta), \\
 \tilde{\Phi}G_{22}^A(k; \eta) &= \frac{\sqrt{\pi} \operatorname{Erf}(y)}{y} \left(\frac{3\Phi_{12}^{(1)}(k; \eta, \eta)}{5} + \frac{2\Phi_{22}^{(1)}(k; \eta, \eta)}{5} \right) \\
 & - \frac{4}{175} \mathcal{B}(y^2) (\Phi_{12}^{(1)}(k; \eta, \eta) - \Phi_{22}^{(1)}(k; \eta, \eta)), \tag{B.4}
 \end{aligned}$$

and

$$\tilde{\Phi}G_{ab}^B(k; \eta) = u_a u_b P^0(k) \left[y^2 (e^{-y^2} - 1) + \sqrt{\pi} y^3 \operatorname{Erf}(y) \right], \tag{B.5}$$

with $y \equiv e^\eta k \sigma_v$. The function $\mathcal{B}(y^2)$ is a combination of generalized hypergeometric functions,

$$\begin{aligned}
 \mathcal{B}(y^2) &\equiv 35 {}_2F_2 \left(\frac{1}{2}, 1; \frac{5}{4}, \frac{7}{4}; -y^2 \right) - 28 {}_2F_2 \left(1, \frac{3}{2}; \frac{7}{4}, \frac{9}{4}; -y^2 \right) \\
 & + 8 {}_2F_2 \left(\frac{3}{2}, 2; \frac{9}{4}, \frac{11}{4}; -y^2 \right). \tag{B.6}
 \end{aligned}$$

Eq. (B.3) gives the large y limit of the third line of eq. (33). In the very large k limit $\Phi_{ab}^{(1)}(k; \eta, \eta) \rightarrow u_a u_b P^0(k) y^2$ and eq. (B.3) goes to eq. (49).

As we have discussed in the text, in the small momentum limit the second term, $\tilde{\Phi}G_{ab}^B(k; \eta)$ has to be switched off, because it contains 2-loop expressions valid at large k . Therefore we will multiply it by a momentum cutoff function. In our numerical implementations, as discussed in the text, we have used the expression

$$\tilde{\Phi}G_{ab}^A(k; \eta) + \frac{\left(\frac{k}{\bar{k}}\right)^4}{1 + \left(\frac{k}{\bar{k}}\right)^4} \tilde{\Phi}G_{ab}^B(k; \eta), \tag{B.7}$$

where $\bar{k} = 0.2 \text{ h/Mpc}$ represents a reasonable value above which the large scale expression can start to be applicable.

The initial conditions must be given at a very large redshift $z_{in} = O(100)$, where the PS can be approximated with the linear one:

$$P_{ab}(k; \eta_{in}) = u_a u_b P^0(k), \tag{B.8}$$

and the equations can then be integrated down to the required final redshift, corresponding to $\eta_f = \log D(z_f)/D(z_{in})$.

References

- [1] F. Bernardeau, S. Colombi, E. Gaztanaga and R. Scoccimarro, *Large-scale structure of the universe and cosmological perturbation theory*, *Phys. Rept.* **367** (2002) 1–248 [astro-ph/0112551].

- [2] **SDSS Collaboration**, D. J. Eisenstein *et. al.*, *Detection of the Baryon Acoustic Peak in the Large-Scale Correlation Function of SDSS Luminous Red Galaxies*, *Astrophys. J.* **633** (2005) 560–574 [[astro-ph/0501171](#)].
- [3] W. J. Percival, R. C. Nichol, D. J. Eisenstein, D. H. Weinberg, M. Fukugita, A. C. Pope, D. P. Schneider, A. S. Szalay, M. S. Vogeley, I. Zehavi, N. A. Bahcall, J. Brinkmann, A. J. Connolly, J. Loveday and A. Meiksin, *Measuring the Matter Density Using Baryon Oscillations in the SDSS*, *Astrophys. J.* **657** (Mar., 2007) 51–55 [[arXiv:astro-ph/0608635](#)].
- [4] E. Gaztanaga, A. Cabre, F. Castander, M. Crocce and P. Fosalba, *Clustering of Luminous Red Galaxies III: Detection of the Baryon Acoustic Peak in the 3-point Correlation Function*, 0807.2448.
- [5] **SDSS Collaboration** Collaboration, B. A. Reid *et. al.*, *Baryon Acoustic Oscillations in the Sloan Digital Sky Survey Data Release 7 Galaxy Sample*, *Mon.Not.Roy.Astron.Soc.* **401** (2010) 2148–2168 [[0907.1660](#)].
- [6] C. Blake, T. Davis, G. Poole, D. Parkinson, S. Brough *et. al.*, *The WiggleZ Dark Energy Survey: testing the cosmological model with baryon acoustic oscillations at $z=0.6$* , 1105.2862.
- [7] S. Nuza, A. Sanchez, F. Prada, A. Klypin, D. Schlegel *et. al.*, *The clustering of galaxies at z 0.5 in the SDSS-III Data Release 9 BOSS-CMASS sample: a test for the Λ CDM cosmology*, 1202.6057.
- [8] A. G. Sanchez, C. Scoccola, A. Ross, W. Percival, M. Manera *et. al.*, *The clustering of galaxies in the SDSS-III Baryon Oscillation Spectroscopic Survey: cosmological implications of the large-scale two-point correlation function*, 1203.6616.
- [9] C. Blake *et. al.*, *The WiggleZ Dark Energy Survey: Joint measurements of the expansion and growth history at $z < 1$* , 1204.3674.
- [10] R. Laureijs, *Euclid Assessment Study Report for the ESA Cosmic Visions*, 0912.0914.
- [11] **Supernova Cosmology Project** Collaboration, S. Perlmutter *et. al.*, *Measurements of Omega and Lambda from 42 High-Redshift Supernovae*, *Astrophys. J.* **517** (1999) 565–586 [[astro-ph/9812133](#)].
- [12] **Supernova Search Team** Collaboration, A. G. Riess *et. al.*, *Observational Evidence from Supernovae for an Accelerating Universe and a Cosmological Constant*, *Astron. J.* **116** (1998) 1009–1038 [[astro-ph/9805201](#)].
- [13] K. Heitmann, M. White, C. Wagner, S. Habib and D. Higdon, *The Coyote Universe I: Precision Determination of the Nonlinear Matter Power Spectrum*, *Astrophys.J.* **715** (2010) 104–121 [[0812.1052](#)].
- [14] M. Pietroni, *Flowing with Time: a New Approach to Nonlinear Cosmological Perturbations*, *JCAP* **0810** (2008) 036 [[0806.0971](#)].
- [15] K. Koyama, A. Taruya and T. Hiramatsu, *Non-linear Evolution of Matter Power Spectrum in Modified Theory of Gravity*, *Phys.Rev.* **D79** (2009) 123512 [[0902.0618](#)].
- [16] R. Scoccimarro, *Large-Scale Structure in Brane-Induced Gravity I. Perturbation Theory*, *Phys.Rev.* **D80** (2009) 104006 [[0906.4545](#)].
- [17] E. Sefusatti and F. Vernizzi, *Cosmological structure formation with clustering quintessence*, *JCAP* **1103** (2011) 047 [[1101.1026](#)].
- [18] S. Anselmi, G. Ballesteros and M. Pietroni, *Non-linear dark energy clustering*, *JCAP* **1111** (2011) 014 [[1106.0834](#)].
- [19] G. D’Amico and E. Sefusatti, *The nonlinear power spectrum in clustering quintessence cosmologies*, *JCAP* **1111** (2011) 013 [[1106.0314](#)].
- [20] M. Crocce and R. Scoccimarro, *Renormalized Cosmological Perturbation Theory*, *Phys. Rev.* **D73** (2006) 063519 [[astro-ph/0509418](#)].
- [21] M. Crocce and R. Scoccimarro, *Memory of Initial Conditions in Gravitational Clustering*, *Phys. Rev.* **D73** (2006) 063520 [[astro-ph/0509419](#)].
- [22] S. Anselmi, S. Matarrese and M. Pietroni, *Next-to-leading resummations in cosmological perturbation theory*, *JCAP* **1106** (2011) 015 [[1011.4477](#)].

- [23] F. Bernardeau and P. Valageas, *Propagators in Lagrangian space*, *Phys.Rev.* **D78** (2008) 083503 [0805.0805].
- [24] F. Bernardeau, M. Crocce and R. Scoccimarro, *Multi-Point Propagators in Cosmological Gravitational Instability*, *Phys.Rev.* **D78** (2008) 103521 [0806.2334].
- [25] K. Skovbo, *Large- k Limit of Multi-Point Propagators in the RG Formalism*, *JCAP* **1203** (2012) 031 [1110.2655].
- [26] S. Matarrese and M. Pietroni, *Resumming Cosmic Perturbations*, *JCAP* **0706** (2007) 026 [astro-ph/0703563].
- [27] A. Taruya and T. Hiramatsu, *A Closure Theory for Nonlinear Evolution of Cosmological Power Spectra*, *Astrophys.J.* **674** (Feb., 2008) 617–635 [0708.1367].
- [28] T. Matsubara, *Resumming Cosmological Perturbations via the Lagrangian Picture: One-loop Results in Real Space and in Redshift Space*, *Phys. Rev.* **D77** (2008) 063530 [0711.2521].
- [29] A. Elia, S. Kulkarni, C. Porciani, M. Pietroni and S. Matarrese, *Modelling the clustering of dark matter haloes in resummed perturbation theories*, *MNRAS* **416** (Sept., 2011) 1703–1716 [1012.4833].
- [30] X. Wang, M. Neyrinck, I. Szapudi, A. Szalay, X. Chen *et. al.*, *Perturbation Theory of the Cosmological Log-Density Field*, *Astrophys.J.* **735** (2011) 32 [1103.2166].
- [31] X. Wang and A. Szalay, *Resummed Perturbation Theory of Galaxy Clustering*, 1204.0019.
- [32] G. Juergens and M. Bartelmann, *Perturbation Theory Trispectrum in the Time Renormalisation Approach*, 1204.6524. 10 pages, 4 figures.
- [33] S. Tassev and M. Zaldarriaga, *Estimating CDM Particle Trajectories in the Mildly Non-Linear Regime of Structure Formation. Implications for the Density Field in Real and Redshift Space*, 1203.5785.
- [34] S. Tassev and M. Zaldarriaga, *The Mildly Non-Linear Regime of Structure Formation*, *JCAP* **1204** (2012) 013 [1109.4939].
- [35] M. Sato and T. Matsubara, *Nonlinear Biasing and Redshift-Space Distortions in Lagrangian Resummation Theory and N -body Simulations*, *Phys.Rev.* **D84** (2011) 043501 [1105.5007].
- [36] D. J. Eisenstein and W. Hu, *Power spectra for cold dark matter and its variants*, *Astrophys.J.* **511** (1997) 5 [astro-ph/9710252].
- [37] S. Pueblas and R. Scoccimarro, *Generation of Vorticity and Velocity Dispersion by Orbit Crossing*, *Phys.Rev.* **D80** (2009) 043504 [0809.4606].
- [38] P. Valageas, *Impact of shell crossing and scope of perturbative approaches in real and redshift space*, *Astron. Astrophys.* **526** (2011) A67 [1009.0106].
- [39] M. Pietroni, G. Mangano, N. Saviano and M. Viel, *Coarse-Grained Cosmological Perturbation Theory*, *JCAP* **1201** (2012) 019 [1108.5203].
- [40] F. Bernardeau, M. Crocce and R. Scoccimarro, *Constructing Regularized Cosmic Propagators*, 1112.3895.
- [41] K. Heitmann, D. Higdon, M. White, S. Habib, B. J. Williams *et. al.*, *The Coyote Universe II: Cosmological Models and Precision Emulation of the Nonlinear Matter Power Spectrum*, *Astrophys.J.* **705** (2009) 156–174 [0902.0429].
- [42] E. Lawrence, K. Heitmann, M. White, D. Higdon, C. Wagner *et. al.*, *The Coyote Universe III: Simulation Suite and Precision Emulator for the Nonlinear Matter Power Spectrum*, *Astrophys.J.* **713** (2010) 1322–1331 [0912.4490].
- [43] A. Lewis, A. Challinor and A. Lasenby, *Efficient Computation of CMB anisotropies in closed FRW models*, *Astrophys. J.* **538** (2000) 473–476 [astro-ph/9911177].
- [44] J. Carlson, M. White and N. Padmanabhan, *A critical look at cosmological perturbation theory techniques*, *Phys. Rev.* **D80** (2009) 043531 [0905.0479].
- [45] S. Saito, M. Takada and A. Taruya, *Impact of massive neutrinos on nonlinear matter power spectrum*, *Phys. Rev. Lett.* **100** (2008) 191301 [0801.0607].
- [46] J. Lesgourgues, S. Matarrese, M. Pietroni and A. Riotto, *Non-linear Power Spectrum including Massive Neutrinos: the Time-RG Flow Approach*, *JCAP* **0906** (2009) 017 [0901.4550].

- [47] S. Saito, M. Takada and A. Taruya, *Nonlinear power spectrum in the presence of massive neutrinos: perturbation theory approach, galaxy bias and parameter forecasts*, *Phys. Rev.* **D80** (2009) 083528 [0907.2922].
- [48] F. Saracco, M. Pietroni, N. Tetradis, V. Pettorino and G. Robbers, *Non-linear Matter Spectra in Coupled Quintessence*, *Phys. Rev.* **D82** (2010) 023528 [0911.5396].
- [49] N. Bartolo, J. P. B. Almeida, S. Matarrese, M. Pietroni and A. Riotto, *Signatures of Primordial non-Gaussianities in the Matter Power-Spectrum and Bispectrum: the Time-RG Approach*, *JCAP* **1003** (2010) 011 [0912.4276].
- [50] F. Bernardeau, M. Crocce and E. Sefusatti, *Multi-Point Propagators for Non-Gaussian Initial Conditions*, *Phys.Rev.* **D82** (2010) 083507 [1006.4656].
- [51] P. McDonald, *Dark matter clustering: a simple renormalization group approach*, *Phys. Rev.* **D75** (2007) 043514 [astro-ph/0606028].
- [52] T. Hiramatsu and A. Taruya, *Chasing the non-linear evolution of matter power spectrum with numerical resummation method: solution of closure equations*, *Phys. Rev.* **D79** (2009) 103526 [0902.3772].
- [53] B. Audren and J. Lesgourgues, *Non-linear matter power spectrum from Time Renormalisation Group: efficient computation and comparison with one-loop*, *JCAP* **1110** (2011) 037 [1106.2607].